Performance Evaluation of Photonic Crystal Fiber for Sensing Applications

by

Sheikh Montasir Mahbub

MASTER OF SCIENCE

IN

ELECTRICAL AND ELECTRONIC ENGINEERING

Department of Electrical and Electronic Engineering
Islamic University of Technology (IUT)
Board Bazar, Gazipur-1704, Bangladesh.

October,2024

Performance Evaluation of Photonic Crystal Fiber for Sensing Applications

by

Sheikh Montasir Mahbub

MASTER OF SCIENCE

IN

ELECTRICAL AND ELECTRONIC ENGINEERING

Department of Electrical and Electronic Engineering
Islamic University of Technology (IUT)
Board Bazar, Gazipur-1704, Bangladesh.

October,2024

CERTIFICATE OF APPROVAL

The thesis titled "**Performance Evaluation of Photonic Crystal Fiber for Sensing Applications**" submitted by Sheikh Montasir Mahbub, bearing student ID 201021022 of Academic Year 2020-21 has been found as satisfactory and accepted as partial fulfillment of the requirement for the Degree MASTER OF SCIENCE IN ELECTRICAL AND ELECTRONIC ENGINEERING on October 04, 2024.

Board of Examiners:

Prof. Dr. Rakibul Hasan Sagor
Professor,
Electrical and Electronic Engineering Department,
Islamic University of Technology (IUT), Gazipur.

Chairman
(Supervisor)

Prof. Dr. Mohammad Rakibul Islam
Professor and Head,
Electrical and Electronic Engineering Department,
Islamic University of Technology (IUT), Gazipur.

Member
(Ex- Officio)

Prof Dr. Md. Ruhul Amin
Pro VC (Acting) and Professor
Electrical and Electronic Engineering Department,
Islamic University of Technology (IUT), Gazipur.

Member

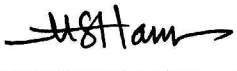

Prof. Dr. Md. Shah Alam
Electrical and Electronic Engineering Department,
Bangladesh University of Engineering and Technology (BUET), Dhaka.

Member
(External)

Declaration of Candidate

It is hereby declared that this thesis report or any part of it has not been submitted elsewhere for the award of any Degree or Diploma.

_____

Prof. Dr. Rakibul Hasan Sagor
Professor,
Electrical and Electronic Engineering Department,
Islamic University of Technology (IUT).
Date: October 04,2024

_____

Sheikh Montasir Mahbub
Student ID:201021022,
Academic Year: 2020-21.
Date: October 04,2024

Praise to Almighty Allah and I dedicate this achievement to my family members.

Table of Contents

List of Figures

List of Tables

ACKNOWLEDGEMENT

I would like to take this opportunity to express my sincere gratitude to all those who have supported me throughout the course of my master's thesis.

First and foremost, I would like to thank Almighty Allah for giving me the mental and physical strength to navigate through the timeline of my master's coursework and thesis. I am grateful to my thesis advisor, Dr. Rakibul Hasan Sagor, for his continuous support, patience, and insightful feedback. His guidance was essential in navigating the challenges of this research, and his expertise greatly contributed to the quality of this thesis.

A special thank you goes to my family for their unconditional love and encouragement. To my parents, thank you for your unwavering support and for instilling in me the values of perseverance and hard work. To my partner and son, your patience, understanding, and constant motivation have been indispensable.

I would also like to acknowledge colleagues of the Department of Electrical and Electronic Engineering (EEE) at Islamic University of Technology (IUT), whose camaraderie and support made this journey enjoyable.

Finally, I would like to thank everyone who directly or indirectly contributed to this thesis. Your support and encouragement have been invaluable, and this achievement is as much yours as it is mine.

Thank you all.

Sheikh Montasir Mahbub
October 2024

ABSTRACT

This research focuses on a novel approach of refractive index sensing by utilizing the nonlinear properties of Hollow Core Photonic Crystal Fibers (HC-PCF) which help ultra-short pulses to get compressed as they propagate through the fiber. The researchers have been working on optical fiber based sensors in recent years but their sensing mechanisms rely on quite a few number of parameters.

In this work, a solution to this problem has been proposed which works quite efficiently. Hollow Core Photonic Crystal Fiber (HC-PCF) filled with either gas or liquid having different refractive indices is exposed to ultra-short pulses. Due to the variation in refractive indices, the fiber characteristic parameters for each testing case appear to be unique. Hence for each case, the ultra-short pulse that has been sent through the fiber changes its shape uniquely as it traverses through the fiber and the power of the output pulse also appears to be non-identical. By analyzing this change in shape and power, the Material Under Sensing (MUS) can be easily detected. In this work, successful sensing of gaseous materials and also liquid materials have been demonstrated.

In terms of gas sensing, as much as 64% compression sensitivity has been achieved alongside 369.07 W of Power Upsurge for CO2 as MUS. Whereas, if the MUS for hollow core photonic crystal fiber is chosen with a higher refractive index within the range of 1.35 – 1.455, as much as 11.6% of compression sensitivity has been achieved with 2313.918W of elevation in Power. This innovative approach holds promise for the detection of a large variety of petrochemical elements, and biological elements with accuracy and reliability.

Chapter 1
OVERVIEW

1.1 Background

In recent times photonics has emerged as one of the most promising technological field that is capable of shaping the future of humankind as it deals with light emission, manipulation and detection. At its core, the main idea of this field is to deal with photons, the elementary particle of light and their interaction with different materials. This phenomenon is now being used in various applied fields ranging from communications systems to healthcare to industrial applications. With the advancement of the technology at our hand, this field is becoming more efficient and has a bigger role to impact the future[1], [2].

Photonics has so far revolutionized different sectors; such as- telecommunication, networking[3]-[5], high speed computing[6]-[8], sensing[9], [10], energy sectors[11], biomedical industries[12], [13] and so on. This evolution of photonics into a mainstream technology began with the discovery of fundamental principles such as total internal reflection and the development of laser technologies in the mid-20th century. Total internal reflection, first theorized by Jean-Daniel Colladon and Jacques Babinet in the 19th century, allowed for the confinement and guidance of light within a medium. Later, the invention of the laser in 1960 by Theodore Maiman provided a coherent and focused light source, sparking a wave of innovation in light-based technologies[14]-[18].

The advancement of optical fibers is a significant milestone in the domain of photonics. In 1966, Sir Charles Kao and George Hockham successfully demonstrated low-loss optical fibers for telecommunications at Standard Telecommunication Laboratories (STL) in Harlow, England[19]. Their pioneering research showed that utilizing purified silica glass enables light transmission across extensive distances with negligible loss. Kao's realization that optical fibers may transform communication ultimately earned him the Nobel Prize in Physics in 2009.

Kao and Hockham's discovery is based on prior investigations on light transmission through fibers. During the 1950s, researchers such as Narinder Singh Kapany established the potential of light transmission through thin fibers, hence proposing the name "fiber optics." However, it was the combination of Kao’s theoretical work on light attenuation and the subsequent advancements in glass purification techniques that allowed optical fibers to become a viable technology for telecommunications[20]-[22].

Optical fibers have become crucial for transmitting information at the speed of light. The advancement of fibers with progressively reduced losses and advancements in lasers, detectors, and signal processing technologies has resulted in optical communication systems capable of transmitting data over continents and seas with minimal distortion. Optical fibers are the backbone of global telecommunications, facilitating high-speed internet, video streaming, and real-time communication, driving the modern information era. In addition to telecommunications, optical fibers have become essential tools in various other domains. One of the most exciting developments is the use of optical fiber-based sensors, which leverage the interaction between light and matter to detect changes in physical, chemical, or biological parameters. These sensors are employed in fields ranging from structural health monitoring and environmental sensing to biomedical diagnostics and industrial applications. Their ability to operate in harsh environments, their immunity to electromagnetic interference, and their high sensitivity make them ideal for a wide range of sensing applications[10]-[12], [23]-[25].

As photonics continues to push the boundaries of what is possible, optical fibers are at the forefront of this transformation. From their beginnings in a lab in England to their current role as the backbone of global communication and advanced sensing technologies, optical fibers, specially as sensors have played a crucial role in shaping the future of technology.

1.2 Optical Fiber-based sensors

Optical fiber-based sensors have proven to be highly versatile tools for detecting physical, chemical, and biological changes across various fields such as structural health monitoring, biomedical diagnostics, environmental sensing, and industrial applications. These sensors utilize the properties of optical fibers to sense changes in external conditions by measuring the interaction of light within or around the fiber. The ability to operate in harsh conditions, along with their immunity to electromagnetic interference, makes them highly effective in many advanced applications.

Optical fiber-based sensors can be categorized into these types-

1. Fiber Bragg Grating (FBG) Sensors

Fiber Bragg Grating (FBG) sensors are one of the most popular and widely used optical fiber sensors. They work by creating periodic changes in the refractive index along the fiber, forming a grating that reflects specific wavelengths of light. When external factors such as strain or temperature are applied to the fiber, these wavelengths shift, allowing precise detection of the applied condition. They are mostly used to monitor local static and fluctuating temperature, refractive index in electrochemical systems, strain, pressure etc[26], [27].

2. Extrinsic Fabry-Perot Interferometer (EFPI) Sensors

EFPI sensors utilize an external Fabry-Perot cavity that creates interference patterns. Any environmental change, such as pressure or strain, causes a shift in these interference patterns, which can be detected through changes in light propagation.

These sensors are commonly used in industrial environments where high sensitivity and robustness are required. EFPI sensors are ideal for sensing gravitational wave, also as optical filters to quantum optomechanics[28], [29].

3. Evanescent Wave Sensors

Evanescent wave sensors take advantage of the evanescent field that extends outside the core of the optical fiber. When the fiber is exposed to the surrounding environment, changes in the refractive index near the fiber's surface affect the evanescent wave, altering light propagation inside the fiber. This interaction is used to detect environmental changes, particularly in liquid or gas mediums. These sensors are primarily used in chemical and biological sensing[30], [31].

4. Distributed Optical Fiber Sensors

Distributed optical fiber sensors use the entire length of the fiber as the sensing element. This enables continuous real-time monitoring along the fiber's entire length. By analyzing the backscattering of light (through effects such as Rayleigh, Raman, or Brillouin scattering), these sensors can detect changes in temperature, strain, or pressure at multiple points along the fiber.

Distributed sensors are ideal for long-distance monitoring, such as in oil and gas pipelines, power transmission lines, and large-scale infrastructure like bridges or railways. They are particularly useful for detecting leaks, structural shifts, or temperature anomalies[32], [33].

5. Surface Plasmon Resonance (SPR) Sensors

SPR sensors utilize the interaction between light and free electrons on the surface of a metal film attached to the fiber. When light hits the metal surface, it excites surface plasmons, and the resulting resonant condition is highly sensitive to changes in the refractive index near the fiber surface. This allows for precise detection of chemical and biological interactions.

SPR sensors are widely used in biochemical sensing for detecting molecular interactions, such as in medical diagnostics, drug testing, and environmental monitoring[34]-[36].

6. Photonic Crystal Fiber (PCF) Sensors

Photonic Crystal Fibers (PCFs) are a class of optical fibers characterized by a periodic arrangement of air holes along the fiber length. These holes create a microstructured cladding that enables unique light-guiding properties. PCF sensors are particularly useful for enhancing light-matter interactions due to the air-filled holes, which can be filled with different materials such as gases, liquids, or even biological samples. This feature makes PCF sensors highly sensitive and ideal for a wide range of sensing applications, particularly where extreme precision is required[37]-[39].

1.3 HC PCF sensors

Among all these types of optical fiber-based sensors, the focus of this thesis has been on PCF sensors, specially on HC-PCF. HC-PCFs represent a significant advancement in optical fiber technology, enabling enhanced control over light propagation due to their unique microstructured design. These fibers consist of a hollow central core surrounded by a periodic arrangement of air holes in the cladding. The hollow core allows light to be guided primarily through air or gas, significantly reducing interaction with the solid material of the fiber. This unique configuration makes HC-PCFs ideal for a wide range of sensing applications, particularly where the interaction of light with external materials is desired[40].

In the context of nonlinear optics, HC-PCFs provide an exceptional platform for studying and utilizing nonlinear effects. The hollow core can be filled with various materials, including gases or liquids with different refractive indices. The combination of high-intensity ultra-short pulses and the nonlinear properties of the filled material produces various effects, such as self-phase modulation (SPM), four-wave mixing (FWM), and soliton generation. These nonlinear effects can be harnessed to detect subtle changes in the material filling the core by observing how the propagation of light is altered[41].

Nonlinear Effects for Material Detection

In this work, the nonlinear properties of the HC-PCF system were utilized by filling the hollow core with materials of varying refractive indices. Ultra-short pulses, typically in the picosecond regime, were sent through the fiber, interacting with the material inside the core. Due to the high intensity of the ultra-short pulses, the light experienced nonlinear effects that modified the pulse as it propagated through the fiber.

The degree and nature of these modifications varied depending on the refractive index of the material filling the core. Materials with different refractive indices produced different levels of pulse compression,

allowing for precise detection and characterization of the materials. The ability to detect these nonlinear-induced changes enabled the identification of the core material based on its unique influence on the ultra-short pulse.

For instance, when the core was filled with a gas of a particular refractive index, the ultra-short pulse underwent noticeable pulse compression due to the nonlinear interactions between the light and the gas[42]. Again, a liquid with a higher refractive index caused stronger pulse compression and more significant temporal reshaping. By analyzing the changes in the pulse characteristics, the material could be detected and identified with a high degree of precision[43], [44].

1.4 Literature Review

The study of HC-PCFs and their nonlinear optical properties has been the subject of significant research over the past few decades. Numerous studies have focused on understanding how ultra-short pulses behave within these unique fibers and how the material filling the hollow core influences light propagation. The research has particularly explored the nonlinear phenomena that arise during light-matter interactions, such as pulse compression, spectral broadening, and soliton formation, which are crucial for applications in sensing and material detection.

Early studies laid the groundwork by exploring the general principles of photonic crystal fibers and their ability to guide light with minimal interaction with the solid core. As technology advanced, research began focusing more on the nonlinear properties of HC-PCFs when filled with various materials, particularly gases and liquids. These studies demonstrated how the refractive index of the core material could influence the nonlinear effects observed in the propagation of ultra-short pulses, offering insights into new sensing mechanisms.

The following table provides an overview of the key papers reviewed during the research for this project. These studies informed the development of the methodology used to explore the nonlinear behavior of ultra-short pulses in HC-PCFs filled with different materials and ultimately inspired the idea to use this effect for precise material detection.

Table 1.1: Contribution of researchers in the field of HC PCF and ultra short pulse propagation through HC PCF

Researcher	Contribution	Year
Gaeta et al. [45]	Studied the potential of nonlinear optics in HC-PCF	2005
Lægsgaard et al. [48]	Presented how ultra short pulses create solitons in a PCF that exhibits transmission based on Photonic Band Gap.	2009
Hu et al. [49]	Exhibited nonlinear optical phenomena like supercontinuum generation in a PCF.	2010
Mosley et al. [62]	Exhibited ultrashort pulse compression and delivery in a hollow-core photonic crystal fiber at a 540 nm wavelength.	2010
Travers et al. [41]	Reviewed how ultra-fast pulses can be transmitted through HC-PCF filled with gas.	2011
Russel et al. [40]	Discussed about utilizing nonlinear properties of a HC-PCF where the core is filled with gas.	2014
Bermudez et al. [47]	Investigated how ultra short pulses create solitons in a PCF	2016
Baharin et al. [56]	Demonstrated an application of hollow-core photonic crystal fiber (HC-PCF) as a refractive index sensor.	2016
Eilzer et al. [52]	Demonstrated how commercial ultra short laser pulse generators can be used in HC-PCF	2018
Markos et al. [54]	Made a review different types of PCF's.	2019
Ahmed et al. [55]	Showcased an application of HC-PCF in the form of refractive index sensor.	2019
Habib et al. [58]	Presented a HC-PCF sensor that works in THz regime and efficiently identifies chemical elements.	2019
Yu et al. [51]	Showcased how HC-PCF can be used a gas sensor	2020
Biswas et al. [46]	Demonstrated how short pulses can be transmitted through fiber that exhibits transmission based on Photonic Band Gap.	2020
Qi et al. [50]	Explored the potential of nonlinear pulse propagation in a Photonic Band Gap Fiber.	2021
Harvey et al. [53]	Reviewed how ultra short pulses in PCF experiences nonlinear optical effect in the form of spectral broadening	2021
Senthil et al. [57]	Showcased an optimized HC-PCF sensor for gas/liquid sensing.	2021

Eid et al. [59]	Introduced an HC-PCF sensor operating in the THz regime, capable of efficiently identifying blood components.	2021
Sardar et al. [60]	Demonstrated an efficient HC-PCF for monitoring carbon dioxide gas.	2021
Khelladi [61]	Reviewed how ultra short pulses behave in PCF's built with different materials.	2022
Saad et al. [90]	Demonstrated recent trends in optical fiber sensors	2023

These papers provide a comprehensive background on the nonlinear behavior of light in hollow-core fibers, particularly when the core is filled with various materials. Their insights helped form the basis of this research, which explores how changes in the material's refractive index within the hollow core affect ultra-short pulse propagation, enabling precise material detection.

Although the literature review revealed several key research gaps in the development and application of HC-PCFs for sensing applications. While significant progress has been made in understanding the nonlinear optical effects in Solid Core PCFs, such as soliton generation and spectral broadening, current research lacks exploring the same properties in HC-PCFs. Also, the sensing applications shown through HC-PCFs lack precision in detecting complex materials using simple and efficient setups. Moreover, there is a significant limitation in the ability to effectively sense both gaseous and liquid substances using a single PCF sensor. Additionally, there is limited exploration of ultra-short pulse interactions with HC-PCF, which could significantly improve sensing accuracy. These gaps underscore the need for novel approaches that leverage nonlinear effects to develop more precise, sensitive, and easily implementable sensing mechanisms, which is the focus of this thesis.

1.5 Thesis Objective

The primary objective of this thesis is to address the existing gaps in this research area by developing a novel method for material sensing based on refractive index variations, utilizing HC-PCFs and ultra-short pulses. The methodology focuses on analyzing the nonlinear effects induced by ultra-short pulse propagation through materials with varying refractive indices. By studying how these pulses are modified, the thesis aims to achieve precise material detection.

Specific Objectives:

- **Utilize Nonlinear Optical Effects**: Investigate how ultra-short pulses interact with the materials inside the hollow core of photonic crystal fibers, and trigger nonlinear optical effects, which result in pulse compression, spectral broadening, self-phase modulation, and other nonlinear effects.

- **Develop a Novel Sensing Mechanism**: Create a reliable sensing mechanism that can detect and characterize materials based on how they modify the shape of the ultra-short pulses. This mechanism will be based on the unique pulse modifications caused by the refractive index of the materials filling the core. Also, explore the potential applications of this sensing method in fields like gas detection, chemical analysis, and biomedical sensing, where precise material characterization is critical.

  The novelty of this method lies in its use of an HC-PCF sensor, where ultra-short pulses will be employed for material sensing which will utilize nonlinear optical effects, ensuring both simplicity and efficiency. Additionally, it features a single sensor capable of detecting both gaseous and liquid substances, significantly enhancing versatility and sensitivity across a wide range of practical applications.

1.6 Thesis Outline

The first chapter of this thesis, Chapter 1, provides a comprehensive introduction to the foundational concepts of optical fibers and photonic crystal fibers (PCFs). It discusses the evolution of these technologies, highlighting significant contributions made by researchers in the field to date. Additionally, this chapter sets the stage by outlining the motivation for this research and the goals of the thesis. An overview of the thesis structure and the key research questions that will be addressed in subsequent chapters is also presented.

Chapter 2 delves into the theoretical framework of ultra-short pulse propagation through HC-PCFs. It begins by explaining the fundamental principles governing the behavior of ultra-short pulses in optical fibers. The chapter then shifts focus to how the unique structure of HC-PCFs interacts with these pulses. Particular attention is given to the nonlinear optical effects and how different parameters; such as- core design, dispersion, and material refractive indices affect the pulse shape. This chapter also investigates how the presence of materials with varying refractive indices inside the hollow core induces changes in the pulse's temporal and spectral characteristics, forming the basis for material sensing.

Chapter 3 describes the numerical methods employed to analyze and simulate the theoretical phenomena discussed in Chapter 2. The chapter outlines the computational tools and algorithms used to model the complex interaction between ultra-short pulses and the material-filled HC-PCFs. Various numerical techniques, such as Split Step Fourier Method (SSFM) simulations and nonlinear Schrödinger equation solvers, are detailed. These methods are critical for understanding the pulse dynamics and validating the theoretical predictions, forming a bridge between theory and experiment.

In Chapter 4, the design and development of a HC-PCF specifically tailored for gas sensing applications is presented. This chapter covers the design process of the HC-PCF, including the selection of materials, geometric configurations, and the optimization of fiber parameters to maximize sensitivity to gaseous substances. The necessary analysis and simulations conducted to evaluate the performance of the fiber design are discussed. Additionally, this chapter illustrates how the designed fiber was successfully implemented in a sensing mechanism, with experimental results showcasing its ability to detect and distinguish gases based on their refractive indices.

Chapter 5 focuses on the detection of materials with refractive indices ranging from 1.4 to 1.45 using the developed HC-PCF sensing system. This chapter explores the behavior of ultra-short pulses as they propagate through the HC-PCF filled with different materials within this refractive index range. The chapter emphasizes the variations in pulse compression, spectral broadening, and other nonlinear effects that arise as a result of these refractive index differences. These effects are used to detect and differentiate between the materials with high precision. Moreover, this chapter highlights potential applications of the developed sensing system in real-world scenarios, such as adulterated fuel detection, where the fiber's sensitivity can identify impurities in fuel by measuring the changes in its refractive index. Chemical detection is another key application, where the fiber sensor can be utilized to monitor chemical compositions in industrial processes, environmental monitoring, and safety systems. The chapter concludes by outlining the benefits and limitations of the current system and provides suggestions for future improvements and broader applications in industry.

Chapter 6 concludes the thesis by providing a summary of the key findings and contributions made through this research. The chapter highlights how the novel approach of using HC-PCFs with ultra-short pulse propagation successfully achieved precise material sensing based on variations in refractive indices. The concluding remarks also revisit the thesis objectives and reflect on the accomplishments in advancing the understanding and application of HC-PCFs in nonlinear optical sensing.

Additionally, future scopes for research and development are outlined, focusing on further optimization of the HC-PCF design for enhanced sensitivity and efficiency in material detection. This chapter also suggests potential extensions of the work, such as exploring more diverse material types, scaling the sensing system for industrial use, and integrating this technology into compact, portable sensing devices for real-time applications in fields such as environmental monitoring, biomedical diagnostics, and industrial process control.

Chapter 2
Pulse Propagation in Fiber

2.1 Maxwell's Equations and Pulse Propagation in Optical Fibers

The study of pulse propagation in optical fibers is crucial for understanding both linear and nonlinear effects. At any given frequency, optical fibers support a finite number of guided modes, with their spatial distribution determined by solutions to the wave equation. These solutions depend on factors such as the fiber's geometry and refractive index profile, influencing how pulses propagate through the core.

Maxwell's equations provide the fundamental theoretical framework for understanding electromagnetic wave propagation, including light, in optical fibers. These equations describe how electric and magnetic fields behave in different media, such as the dielectric core and cladding of an optical fiber, and how these fields interact to produce wave propagation. This theory is essential for comprehending both the linear and nonlinear dynamics that govern light transmission in optical fibers.

2.1.1 Overview of Maxwell's Equations

Maxwell's equations consist of four partial differential equations that explain how electric fields ($\vec{\boldsymbol{E}}$) and magnetic fields ($\vec{\boldsymbol{H}}$) are generated and evolve over time in the presence of charges and currents. In the context of optical fibers, these equations can be simplified under the assumption that the medium is non-conductive (dielectric), such as glass or silica, and there are no free charges or currents. The four Maxwell's equations are:

Gauss's Law for Electricity:

$$\nabla . \boldsymbol{E} = \frac{\rho}{\epsilon_0} \tag{2.1}$$

This law indicates that the electric flux emanating from a closed surface is proportional to the total electric charge enclosed within the surface. In optical fibers, the medium is typically charge-free, so $\rho = 0$, simplifying this equation to:

$$\nabla . \boldsymbol{E} = 0 \tag{2.2}$$

This implies that the electric field has no divergence, which is significant in guiding the electric field along the fiber's axis.

Gauss's Law for Magnetism:

$$\nabla . \boldsymbol{B} = 0 \tag{2.3}$$

Gauss's law for magnetism states that there are no magnetic monopoles, meaning magnetic field lines do not begin or end at any point but instead form closed loops. This is crucial for understanding the behavior of the magnetic field in relation to the electric field in the optical fiber.

Faraday's Law of Induction:

$$\nabla \times \boldsymbol{E} = -\frac{\partial \boldsymbol{B}}{\partial t} \tag{2.4}$$

Faraday's law explains that a time-varying magnetic field generates a circulating electric field. This principle is central to the propagation of electromagnetic waves in optical fibers. In the context of optical fibers, a changing magnetic field produces an electric field, which, in turn, propagates the light wave forward through the fiber.

Ampère's Law (with Maxwell's correction):

$$\nabla \times \boldsymbol{H} = \boldsymbol{J} + \epsilon_0 \frac{\partial \boldsymbol{D}}{\partial t} \tag{2.5}$$

Ampère's law states that a time-varying electric field can induce a magnetic field, even in the absence of an electric current ($\boldsymbol{J} = \boldsymbol{0}$ in dielectric materials). Therefore, in the case of optical fibers, the equation simplifies to:

$$\nabla \times \boldsymbol{H} = \epsilon_0 \frac{\partial \boldsymbol{D}}{\partial t} \tag{2.6}$$

This relationship between electric and magnetic fields forms the basis for electromagnetic wave propagation in fibers[63].

2.1.2 Application to Optical Fibers

To apply Maxwell's equations to the study of light propagation in optical fibers, the equations must be expressed in a manner that accounts for the fiber's geometry. Optical fibers have a cylindrical structure with a high refractive index core surrounded by a lower refractive index cladding, guiding light primarily through total internal reflection.

For this reason, Maxwell's equations are often expressed in cylindrical coordinates (r, φ, z)) to match the fiber's symmetry. This leads to a system of coupled differential equations that describe the electric and magnetic field components (E_r, E_φ, E_z) and (H_r, H_φ, H_z) inside the fiber.

In cylindrical coordinates, Maxwell's equations describe the interaction between the electric and magnetic fields as they propagate along the fiber axis (the z-direction). The behavior of the fields is determined by the fiber's refractive index profile, which influences how light is confined and guided within the core.

2.2 The Wave Equation for Optical Fiber Propagation

By manipulating Maxwell's equations, the wave equation can be derived, which governs the propagation of electromagnetic waves in a medium. Starting with Faraday's and Ampère's laws and applying the curl operation, the following wave equation for the electric field ($\vec{\boldsymbol{E}}$) in a dielectric medium can be obtained:

$$\nabla^2 \boldsymbol{E} - \mu\epsilon \frac{\partial^2 \boldsymbol{E}}{\partial t^2} = 0 \tag{2.7}$$

Here:

- ∇^2 is the Laplacian operator, describing the spatial variation of the electric field.
- μ is the permeability of the material.
- ϵ is the permittivity of the material.

For optical fibers, μ and ϵ are material constants that vary between the core and the cladding. The above equation describes how the electric field evolves over time and space as it propagates through the fiber.

Similarly, a corresponding wave equation can be derived for the magnetic field ($\vec{\boldsymbol{H}}$). These coupled wave equations are the foundation for understanding light propagation in optical fibers, leading to solutions known as modes[63].

2.3 Fiber Modes

The modes of an optical fiber are the stable field distributions that can propagate down the fiber without changing their shape, apart from possible phase shifts. These modes are solutions to the wave equation subject to the boundary conditions imposed by the fiber's refractive index profile and geometry.

In cylindrical optical fibers, the modes are typically classified into different types based on their field distribution:

- **Transverse Electric (TE) modes**: No longitudinal component of the electric field.
- **Transverse Magnetic (TM) modes**: No longitudinal component of the magnetic field.
- **Hybrid modes (HE and EH)**: Both electric and magnetic fields have longitudinal components.

- **Linearly Polarized (LP) modes**: An approximation used in fibers with a small refractive index difference between core and cladding, where the fields are almost linearly polarized.

The fundamental mode, HE11, is the most important in single-mode fibers. It has the simplest field distribution and is responsible for the majority of light transmission in single-mode fibers used in optical communication.

2.3.1 Single-Mode Condition

For single-mode fibers, the fiber is designed such that only the fundamental HE11 mode propagates. This is achieved by controlling the core radius and the difference in refractive index between the core and the cladding. The condition for single-mode operation is expressed through the V-number or normalized frequency parameter, given by:

$$V = \frac{2\pi}{\lambda} r \sqrt{{n_1}^2 - {n_2}^2} \tag{2.8}$$

Where:

- r is the core radius.
- λ is the operating wavelength of the light.
- n_1 and n_2 are the refractive indices of the core and cladding, respectively.

When the V-number is below a critical value (approximately 2.405), only the fundamental mode (HE11) can propagate. This ensures minimal signal loss and distortion, making single-mode fibers ideal for high-speed optical communication [63].

2.4 Nonlinear Effects and Pulse Propagation

Maxwell's equations are also essential for describing nonlinear optical effects, which become significant when high-intensity light pulses propagate through optical fibers. In nonlinear media, the refractive index depends on the light intensity, leading to effects such as self-phase modulation (SPM), cross-phase modulation (XPM), four-wave mixing (FWM), and Raman scattering. These nonlinear effects cause changes in the pulse shape and spectrum, contributing to phenomena such as spectral broadening and pulse compression.

In fibers, these effects are particularly important when ultra-short pulses (such as femtosecond or picosecond pulses) are used, as their high peak power enhances nonlinear interactions. These nonlinear

effects are exploited in various applications, including optical sensing, where the changes in pulse properties can be used to detect and characterize materials based on their interaction with light.

2.5 Dispersion in Optical Fibers

Maxwell's equations also explain the phenomenon of dispersion, where different frequency components of a pulse travel at different velocities, leading to pulse broadening over long distances. Dispersion is a critical factor in designing optical communication systems because it limits the data transmission rate by causing overlapping of pulses [63],[64].

In optical fibers, dispersion arises from two main sources:

- **Material Dispersion**: Happens due to the dependence on wavelength of the refractive index of the fiber material.
- **Waveguide Dispersion**: Caused by the geometry of the fiber and the distribution of light between the core and cladding.

Managing dispersion is crucial for maintaining signal integrity over long-distance fiber optic networks.

2.6 Nonlinear Wave Equation: Understanding Pulse Propagation in Optical Fibers

The propagation of light pulses through optical fibers is governed by complex interactions between dispersive and nonlinear effects. Understanding these interactions is critical for many applications, including telecommunications, optical sensing, and ultrafast signal processing. When high-intensity light pulses, such as ultra-short pulses (with widths in the femtosecond to picosecond range), propagate through an optical fiber, both linear and nonlinear phenomena shape the pulse's evolution. The nonlinear wave equation, derived from Maxwell's equations, provides a theoretical framework to describe these effects and predict how pulses will behave in different fiber conditions.

This chapter explores the derivation and significance of the nonlinear wave equation, focusing on the impact of group velocity dispersion (GVD), nonlinear effects like the Kerr effect, and how these interact with parameters such as effective refractive index and effective area in fibers. Together, these factors govern the transmission and manipulation of light pulses, determining the efficiency and stability of optical communication systems and advanced sensing mechanisms.

2.6.1 The Fundamental Wave Equation

The propagation of light through any medium, including optical fibers, is fundamentally governed by **Maxwell's equations**, which describe how electric and magnetic fields evolve in space and time. The general wave equation, derived from these fundamental principles, describes how electromagnetic waves (including light) propagate in a medium:

$$\nabla^2 \boldsymbol{E} - \frac{1}{c^2}\frac{\partial^2 \boldsymbol{E}}{\partial t^2} = \mu_0 \frac{\partial^2 \boldsymbol{P}_L}{\partial t^2} + \mu_0 \frac{\partial^2 \boldsymbol{P}_{NL}}{\partial t^2} \tag{2.9}$$

Where:

- $\boldsymbol{E}$ is the electric field,
- $\boldsymbol{P}_L$ and $\boldsymbol{P}_{NL}$ represent the linear and nonlinear polarizations, respectively,
- c is the speed of light in vacuum, and
- μ_0 is the permeability of free space.

For typical optical fibers made of materials like silica, the nonlinear polarization $\boldsymbol{P}_{NL}$ arises primarily from the Kerr effect, where the refractive index of the material becomes dependent on the light intensity. This effect causes self-modulation of the phase of the propagating light wave, leading to significant changes in the pulse characteristics over distance[63],[66].

2.6.2 Nonlinear Polarization and Kerr Effect

The Kerr effect is one of the most significant nonlinear phenomena in optical fibers. It describes how the refractive index of the fiber material increases with the intensity of the light passing through it. Mathematically, the refractive index n of the fiber is expressed as:

$$n = n_0 + n_2 I \tag{2.10}$$

Where:

- n_0 is the linear refractive index,
- n_2 is the nonlinear refractive index coefficient,
- I is the intensity of the light.

This intensity-dependent refractive index results in self-phase modulation (SPM)**,** a process that induces a nonlinear phase shift across the pulse. SPM leads to spectral broadening, which is particularly important in applications such as supercontinuum generation and optical sensing[63],[66].

The nonlinear polarization responsible for the Kerr effect is given by:

$$\boldsymbol{P}_{NL} = \epsilon_0 \chi^{(3)} E^3 \tag{2.11}$$

Where:

- ϵ_0 is the permittivity of free space,
- $\chi^{(3)}$ is the third-order nonlinear susceptibility of the medium.

This equation represents the fact that the polarization is a nonlinear function of the electric field, and as the intensity of the light increases, so does the effect on the refractive index[63],[66].

2.7 Slowly Varying Envelope Approximation (SVEA)

To simplify the analysis of pulse propagation, especially for ultra-short pulses, we use the slowly varying envelope approximation (SVEA). This approximation assumes that the optical field can be represented as a rapidly oscillating carrier wave modulated by a slowly varying envelope. The electric field can be expressed as:

$$E(r,t) = \frac{1}{2}\hat{x}\{E(r,t)e^{-i\omega_0 t} + c.c\} \tag{2.12}$$

Where:

- $E(r,t)$ is the slowly varying envelope of the pulse,
- ω_0 is the carrier frequency,
- $c.c$ denotes the complex conjugate

Substituting this expression into the general wave equation allows us to focus on the dynamics of the envelope, rather than tracking the fast oscillations of the carrier wave. This leads to the derivation of the Nonlinear Schrödinger Equation (NLSE), which describes the evolution of the slowly varying pulse envelope as it propagates through the fiber[63],[66].

2.8 Nonlinear Schrödinger Equation (NLSE)

The Nonlinear Schrödinger Equation (NLSE) is a key equation in fiber optics that describes how optical pulses evolve in the presence of both dispersion and nonlinearity. The NLSE can be written as:

$$\frac{\partial A(z,t)}{\partial z} = -j\frac{\beta_2}{2}\frac{\partial^2 A(z,t)}{\partial T^2} + \frac{\beta_3}{6}\frac{\partial^3 A(z,t)}{\partial T^3} - \frac{\alpha}{2}A(z,t) - j\gamma|A(z,t)|^2 A(z,t) \tag{2.13}$$

Where:

- $A(z,t)$ is the slowly varying envelope of the pulse,
- β_3 is the third-order dispersion term (related to group velocity),
- β_2 is the group velocity dispersion (GVD) coefficient,

- γ is the nonlinear coefficient, related to the effective area A_{eff} the third-order susceptibility $\chi^{(3)}$.
- α is the loss coefficient of the fiber.

This equation accounts for both the dispersive effects, represented by the second-order derivative in time β_2 and the nonlinear effects, represented by the term involving $\gamma|A(z,t)|^2$[63],[66].

2.9 Dispersion Coefficient and Group Velocity Dispersion (GVD)

The term β_2 in the NLSE represents group velocity dispersion (GVD), which accounts for the different velocities at which different frequency components of the pulse travel. GVD can lead to pulse broadening or compression, depending on the sign of β_2. For example:

- Positive GVD (β_2>0) leads to pulse broadening as lower frequencies travel faster than higher frequencies.
- Negative GVD (β_2<0) causes pulse compression.

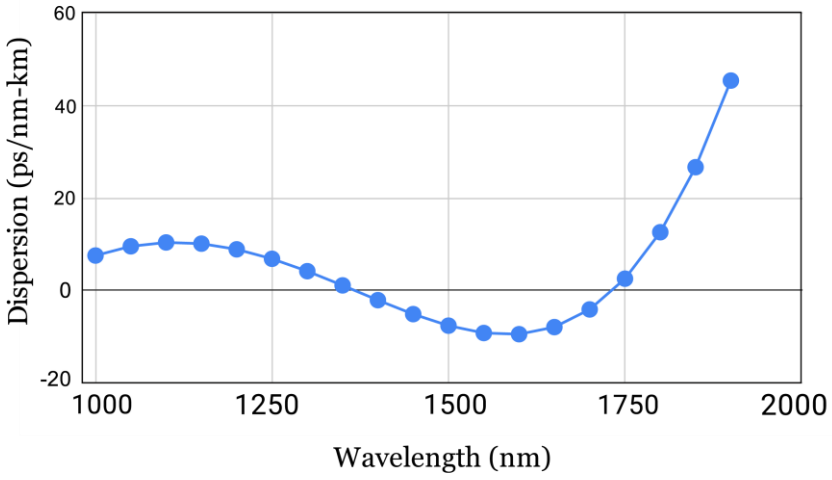

Figure 2.1: Wavelength vs Dispersion graph of an HC-PCF filled with CO_2.

The dispersion coefficient D is related to β_2 by:

$$D = -\frac{2\pi c}{\lambda^2}\beta_2 \tag{2.14}$$

Where, λ is the operating wavelength. Managing dispersion is critical for long-distance optical communication to avoid signal distortion and overlap between consecutive pulses[63],[66].

2.10 Effective Refractive Index

The effective refractive index (n_{eff}) is an important parameter in optical fibers, especially when dealing with guided modes. It describes how light behaves in the core region of the fiber compared to free-space

propagation. The effective refractive index depends on the geometry of the fiber, the core and cladding materials, and the wavelength of light.

In the context of nonlinear optics, the effective refractive index determines the phase velocity of the light pulse as it propagates through the fiber. The phase mismatch between different frequency components (caused by the refractive index's wavelength dependence) contributes to dispersion effects, influencing the shape and behavior of the pulse[63],[66].

2.11 Effective Area

The effective area (A_{eff}) plays a crucial role in determining the strength of nonlinear interactions in optical fibers. It quantifies the cross-sectional area over which the light is confined in the fiber. The nonlinear coefficient γ is inversely proportional to the effective area:

$$\gamma = \frac{n_2 \omega_0}{c\, A_{eff}} \tag{2.15}$$

Where:

- n_2 is the nonlinear refractive index,
- ω_0 is the central frequency,
- A_{eff} is the effective mode area.

A smaller effective area leads to stronger nonlinear effects, making the fiber more sensitive to phenomena like self-phase modulation (SPM) and four-wave mixing (FWM).

The nonlinear wave equation is a crucial tool for understanding the behavior of optical pulses in fibers, particularly when both nonlinear and dispersive effects are present. The Nonlinear Schrödinger Equation (NLSE) captures the essential physics of pulse propagation, showing how dispersion and nonlinearity interact to shape the pulse as it travels. Key parameters such as the dispersion coefficient (D), effective refractive index (n_{eff}), and effective area (A_{eff}), β_1, β_2, γ determine the strength and behavior of these effects, offering valuable insight for designing optical fibers for communication and sensing applications[63], [64], [66].

Chapter 3
Overview of the Simulation and Numerical Analysis

The key objective of this dissertation is to establish a novel approach for refractive index sensing through a HC-PCF. Unlike the existing sensing techniques, the proposed technique makes decision by analyzing the shape of the ultra-short pulses at the receiving end of the HC-PCF. When the hollow core of PCF is filled with either gaseous materials or different samples having refractive indices ranging from 1.4-1.45, the effective refractive indices for each case will be unique ranging in the wavelength from 1000 nm - 2200 nm. This eventually results in distinct optical parameters such as Propagation Constant (β_2, β_3), Dispersion (D), Effective Area (A_{eff}), and Nonlinear Parameter (γ) for each fuel sample. These distinct values of optical parameters will define how the ultra-short pulse will change its shape as it traverses through the HC PCF. Since the parameters will exhibit unique values for each fuel sample, the change in pulse shape will be different for each sample. By observing that change in the form of compression sensitivity and power upsurge, the sensing decision can be made. This novel technique provides highly accurate and sensitive results as well as this approach having a simpler proposed experimental setup.

3.1 Design and Simulation

The primary task was to design a HC-PCF, that can guide light efficiently through it. Initially, the design idea was taken from Thorlabs, a company that produces HC-PCF commercially. HC-PCF generally is a fiber which has a hollow core, surrounded by air holes embedded into silica[67]. The measurements were defined from the commercially available HC-PCF's and then designed in COMSOL Multiphysics.

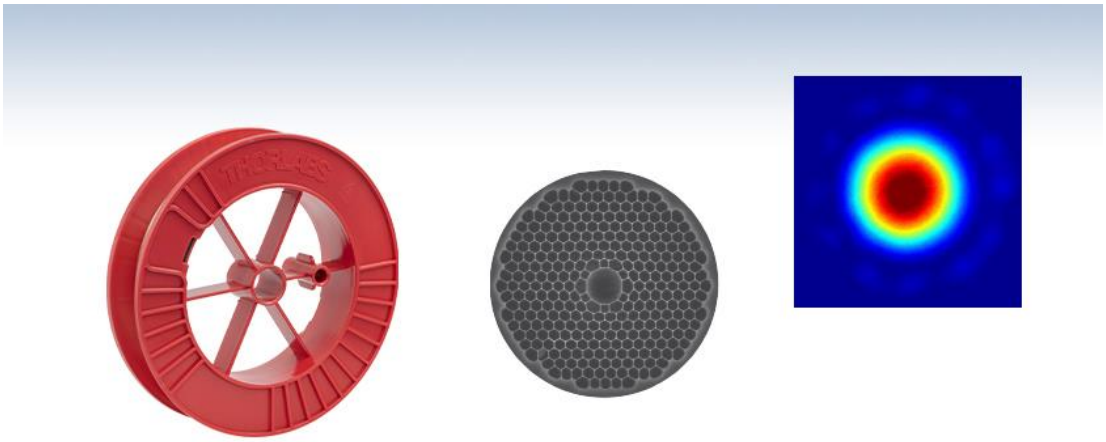

Figure 3.1: HC-PCF samples of THORLABS.

Two HC-PCF's have been designed, one that is capable of detecting gaseous material and another capable of materials having refractive indices within the range of 1.4 to 1.45. For both of the cases, the design is same, some measurements have been changed.

The HC-PCF that has been designed has a hollow core and it is surrounded by 6 layers of elliptical air holes. The gaps between the layers also kept different to maximize the photonic band gap and let the maximum amount of light pass through the core.

The proposed fiber for gas detection has a diameter of 115 µm, a core diameter of 20 µm, and a Perfectly Matched Layer with a width of 7.5 µm. The structure design comprises six layers, comprising circular and elliptical pores. The starting layer is composed of circular holes with a radius of 2.5 µm, spaced 30 degrees apart. The second and fourth layers are composed of ellipses with a major axis length of 3.75 µm and a minor axis length of 2.5 µm. The ellipses of the second layer are arranged 30 degrees apart, while the ellipses of the fourth layer are positioned 15 degrees apart. The subsequent layers are constructed using ellipses with a major axis length of 3.75 µm and a minor axis length of 3.125 µm. Ellipses of the 3rd, 5th, and 6th layers have been set 20°, 12.5°, and 10° apart, respectively. The interlayer spacing between the first and second layers, third and fourth layers, and fifth and sixth layers is maintained at 2.5µm, while the spacing between the second and third layers and the fourth and fifth layers is set at 5µm[42].

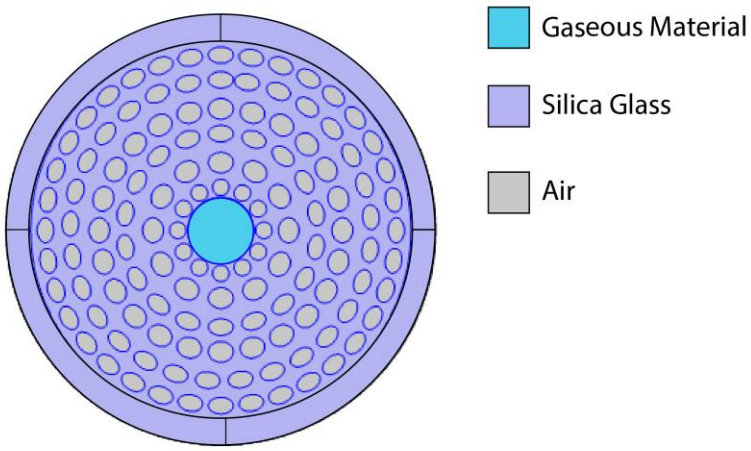

Figure 3.2: Designed HC-PCG structure on COMOSL interface.

The fiber designed for materials having refractive indices within 1.4-1.45, possesses an overall diameter of 20µm and a core diameter of 3.33µm. The air holes are also strategically positioned in six layers around the core. The first layer consists of circular air holes, each with a diameter of 0.83µm, arranged in a circular pattern 30° apart. The subsequent five layers contain elliptical air holes in two distinct configurations: one with a major axis of 0.625µm and a minor axis of 0.42µm, and another with a major axis of 0.625µm and a

minor axis of 0.52µm. The second and fourth layers contain the first type of elliptical holes, spaced 30° and 15° apart, respectively. The second type is placed in the third, fifth, and sixth layers, with spacing at 20°, 12.5°, and 10° apart, respectively. Additionally, a perfectly matched layer with a width of 1.25µm has been incorporated to prevent reflection of the applied light wave back into the system[43].

Using Comsol, the feasibility of the designed HC-PCF's was tested. The software uses Maxwell's equations to calculate the effective refractive index of the HC-PCF over a range of wavelengths.

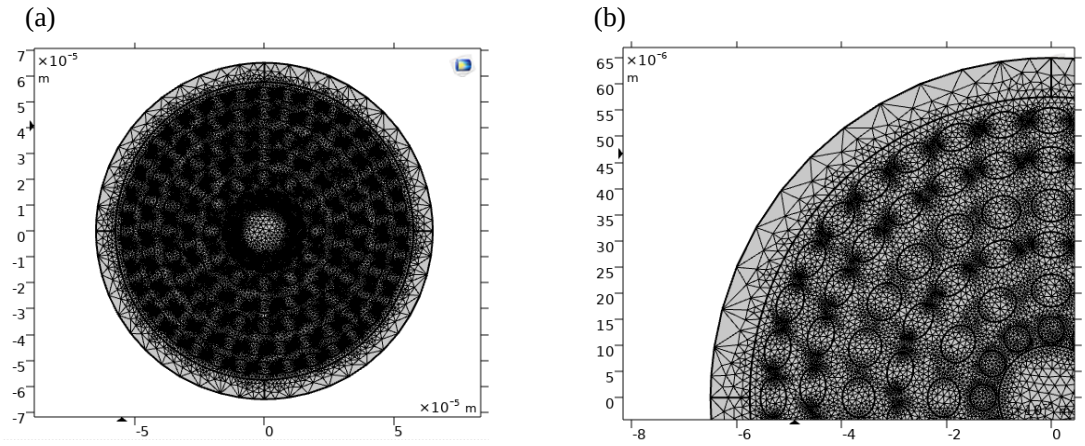

Figure 3.3: a) Finer mesh size applied to the designed HC-PCF (whole structure), b) Clear depiction of finer mesh size applied to the HC-PCF.

Initially, the goal was to identify optical modes where most of the light is confined within the hollow core, a key characteristic for optimizing the HC-PCF's design. To achieve this, the power fraction[58] was calculated using the following equation:

$$Power\ Fraction = \frac{\int_{sample} R_e\left(E_x H_y - E_y H_x\right) dxdy}{\int_{total} R_e\left(E_x H_y - E_y H_x\right) dxdy} \times 100\ \% \tag{3.1}$$

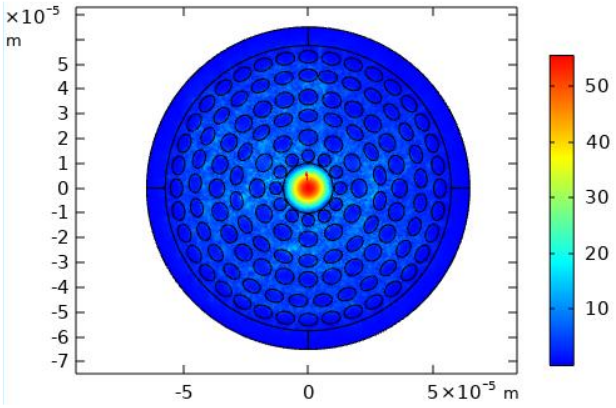

Figure 3.4: Light confinement in designed HC-PCF filled with gas.

As highlighted earlier, the parameters essential for calculating pulse compression are inherently linked to the effective refractive index. After obtaining the effective refractive index from the modal analysis, other critical parameters, such as the Effective Area (A_{eff}), Dispersion coefficient (D), and the Non-linear Parameter (γ), were calculated using the following equations:

- **Effective Area (A_{eff})**,

$$A_{eff} = \frac{(\int |E(x,y)|^2 \, dxdy)^2}{\int |E(x,y)|^4 \, dxdy} \tag{3.2}$$

This expression for the effective area is essential in determining the fiber's non-linear characteristics, as smaller values of A_{eff}, indicate stronger non-linear effects[60].

- **Dispersion Coefficient (D)**,

$$D = \frac{d\,\beta_1}{d\lambda} = -\frac{2\pi c}{\lambda^2}\,\beta_2 \tag{3.3}$$

The dispersion parameter D is directly related to the group velocity dispersion and nth-order dispersion term (β_1, β_2 , and β_3, which, in turn, depend on the effective refractive index, which can be seem from equation 3.4 and 3.5. Accurate calculation of D is critical for understanding how pulse broadening or compression occurs as light propagates through the fiber.

$$\beta_0 = \frac{\omega_0}{c_0}\eta_{\omega_0} \tag{3.4}$$

$$\beta_n = \frac{d}{d\omega}\,\beta_{n-1} \tag{3.5}$$

These constants describe the relationship between the frequency (ω) and the effective refractive index at various orders, capturing the fiber's dispersive properties at different wavelengths[63].

- **Non-linear Parameter (γ)**

$$\gamma = \frac{2\pi}{\lambda}\,\frac{n_2}{A_{eff}} \tag{3.6}$$

The non-linear parameter γ measures the fiber's non-linear response to high-intensity light, which is vital in applications such as supercontinuum generation and pulse compression. It depends on the non-linear refractive index n_2 and the effective area A_{eff}.

Thus, by calculating the effective refractive index through COMSOL, a comprehensive set of fiber characteristics was obtained, forming the foundation for further analysis of pulse propagation, compression, and non-linear effects in the designed HC-PCF. These calculations provide a clear understanding of how

the fiber will perform under various conditions, allowing for fine-tuning of the design to achieve optimal performance[63], [64], [66].

3.2 Solving NLSE

The focus has been on figuring out how the shape of ultra-short pulses changes as they propagate through the designed HC-PCFs, which can only be observed by solving the nonlinear Schrödinger's equation (NLSE).

$$\frac{\partial A}{\partial z} = -j\frac{\beta_2}{2}\frac{\partial^2 A}{\partial T^2} + \frac{\beta_3}{6}\frac{\partial^3 A}{\partial T^3} - \frac{\alpha}{2}A - j\gamma|A|^2 A \tag{3.7}$$

Here,

- A represents the slowly varying pulse envelope,
- z is the propagation distance,
- β_2 is the group-velocity dispersion (GVD) parameter, and
- γ accounts for fiber nonlinearity.

For this particular case, the analytical solution of this equation is quite a daunting task. Instead, a numerical solution using MATLAB, implementing the Split Step Fourier Method (SSFM), is employed. The method works by assuming that the effects of dispersion and nonlinearity can be separated over a small propagation step, *h*, and applied sequentially at each step. To implement SSFM on NLSE, the NLSE can be written in operator form as-

$$\frac{\partial A}{\partial z} = \left(\widehat{D} + \widehat{N}\right)A \tag{3.8}$$

In this formulation,

$$\widehat{D} = -j\frac{\beta_2}{2}\frac{\partial^2 A}{\partial T^2} + \frac{\beta_3}{6}\frac{\partial^3 A}{\partial T^3} - \frac{\alpha}{2}A \tag{3.9}$$

represents the linear effects of dispersion and loss,

while

$$\widehat{N} = j\gamma\{|A|^2 + \frac{j}{\omega_0}\frac{1}{A}\frac{\partial}{\partial T}(|A|^2 A)\} - T_R\frac{\partial|A|^2}{\partial T}z \tag{3.10}$$

models the nonlinear impact on pulse propagation.

In reality, dispersion and nonlinearity act simultaneously as light propagates through the fiber. However, SSFM approximates this process by dividing the propagation distance into small steps, h, and assuming that over each step, the dispersive and nonlinear effects can be applied sequentially.

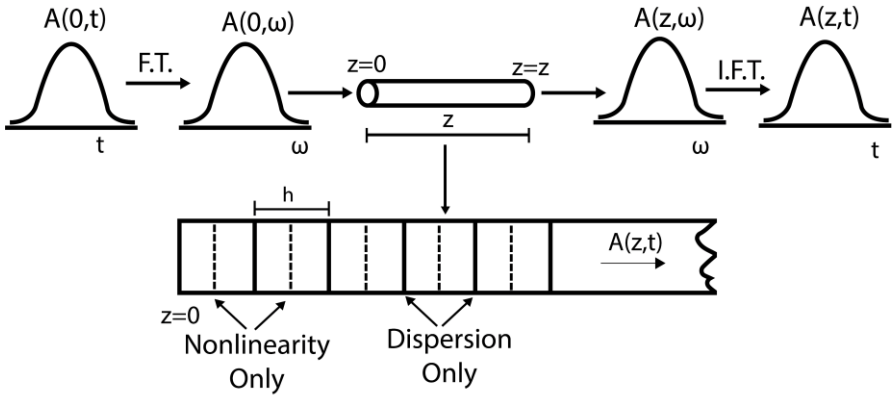

Figure 3.5: Schematic representation of the solution process for the nonlinear Schrödinger equation using the Split-Step Fourier Method (SSFM).

To approximate the evolution of the pulse from position z to z+h, SSFM assumes that the nonlinear effects act first, followed by the dispersive effects, or vice versa. Mathematically, the propagation over a small step can be described as:

$$A(jh,T) \approx e^{h\hat{D}} e^{h\hat{N}} A((j-1)h,T) \tag{3.11}$$

Since the dispersive and nonlinear steps need to be treated independently, the exponential should be split into the product of the dispersive and nonlinear components. However, these operators do not commute, hence the use of the Baker-Hausdorff formula is required-

$$e^{h\hat{D}} e^{h\hat{N}} \approx e^{h(\hat{D}+\hat{N})+\frac{h^2}{2}[\hat{D}+\hat{N}]+\frac{h^3}{12}[\hat{D}-\hat{N},[\hat{D},\hat{N}]]+\cdots} \tag{3.12}$$

As a result, if only the first term is considered, the split-Fourier formula is derived. This accounts for the method's second-order accuracy in terms of h. The accuracy can be further improved by propagating the dispersion for half a step, then applying the nonlinearity at the midpoint, followed by another half-step of dispersion(*Figure 3.5*). This approach is referred to as the symmetric Split-Step Fourier method, which eventually turn the solution of *equation 3.11* to this-

$$A(jh,T) \approx e^{\frac{h}{2}\hat{D}} e^{\int_{(j-1)h}^{jh} \hat{N}(z)dz} e^{\frac{h}{2}\hat{D}} A((j-1)h,T) \tag{3.13}$$

The nonlinear operator is approximated by calculating $h\hat{N}$ at the midpoint, and as long as h is small enough, the error remains minimal. For the dispersion part, it is applied for half a step ($\frac{h}{2}$) both before and after the nonlinear operator. A Fourier transform (FFT) is used to handle the dispersion for that half-step, followed

by an inverse Fourier transform to convert the pulse back to the time domain. This process is straightforward, as illustrated in *Figure 3.5*.

The Fast Fourier Transform (FFT) is applied as an efficient method for performing the Fourier transform, but it operates optimally under specific conditions. The input function must be zero-centered and discretized into a vector with a length that is a power of two, such as 2^a. In this case, 2^{11} points are used for the time domain.

However, there is a limitation. Since the FFT is a discrete Fourier transform, improper selection of windowing parameters can result in aliasing, where overlapping signals distort the results. The number of points and the time step define the width of the time and frequency windows.

In this simulation, the time step of 0.05 times the initial pulse width was chosen. This ensures that both the temporal broadening (due to dispersion) and the spectral widening (due to nonlinear effects) are accurately captured without introducing aliasing. Depending on the scenario, different parameters may be selected to avoid aliasing and maintain accurate representations of both temporal and spectral profiles [63], [64], [65], [66].

All these procedures of SSFM have been translated into a MATLAB code and analysis was done on the ultra short pulse travelling through the designed HC-PCF's. When an ultra-short pulse is introduced at one end of the HC-PCF, its evolution during transmission has been studied using this approach. Various input signal configurations were tested, each with a carefully chosen fiber length. These lengths were determined through extensive analysis to ensure the solution number (N) remains above 1 and that the fiber length is kept within limits, specifically shorter than the fission length ($L_{fission}$).

$$L_{fission} = \frac{L_D}{N} \tag{3.14}$$

Where, L_D is Dispersion length and N is soliton number, they can be calculated using this –

$$L_D = \frac{{T_0}^2}{\text{abs}\,(\beta_2)} \tag{3.15}$$

$$N = \sqrt{\frac{\gamma\, P_0 {T_0}^2}{\beta_2}} \tag{3.16}$$

Where, T_0 is the pulse width of the input pulse and P_0 is the power of the input pulse.

The fission length is defined as the distance at which the pulse starts losing its initial shape, thus it's imperative to maintain the fiber length within this limit. Also, for the pulse to undergo compression, it's essential to have a Soliton Number greater than 1.

Chapter 4
HC-PCF as Gas Sensor and its Performance Analysis

Gas sensing plays a crucial role in a wide range of industries, such as petroleum, chemical manufacturing, environmental monitoring, and healthcare [68],[69],[70]. Traditionally, electronic and chemical sensors have been utilized due to their affordability. However, these methods face inherent challenges, particularly regarding sensitivity, signal interference, and selectivity, which can affect their overall effectiveness.

In contrast, optical fiber sensors operate on a different mechanism, relying on the interaction between light and the fiber. The sensing process involves tracking changes in light parameters, such as phase and intensity, as well as variations in fiber characteristics as light travels through it. Also, different gases exhibit unique refractive indices, they produce distinct optical properties, utilizing this distinct optical properties, the sensing process can be made more precise. Additionally, because optical fibers do not chemically interact with the gases, the issue of selectivity is mitigated [71],[72].

Originally introduced in the 1960s for communication purposes, optical fibers have since evolved to be integral in sensing technologies. In recent years, gas sensing applications have focused on D-shaped solid core fibers [73],[74] and photonic crystal fibers[51]. Among these, hollow-core photonic crystal fiber (HC-PCF) has emerged as a promising technology for gas sensing, despite its unique operating principles. This dissertation presents a novel approach to gas sensing using HC-PCF.

4.1 Design and Simulation

An HC-PCF has been meticulously designed to detect and analyze gaseous materials. The fiber structure predominantly comprises silica glass, which forms the outer framework, while the hollow regions within the fiber are filled with air, except for the central core. This core acts as the primary sensing region, where the specific gas or material under test (MUT) is introduced. This design offers a significant advantage by isolating the test material in the core, which enhances sensitivity and allows for better control over the interaction between light and gas. Additionally, since the hollow regions minimize the contact between the fiber material and the gas, issues like chemical reactions or contamination are effectively mitigated.

The physical dimensions of the fiber closely align with commercially available fibers, specifically those provided by Thorlabs[67]. The proposed HC-PCF features an outer diameter of 115μm, while the core region, which is central to the gas sensing process, has a diameter of 20μm. These dimensions ensure that the fiber is compatible with standard equipment and facilitates easier integration into existing optical

systems, making it suitable for a wide range of practical gas sensing applications. A Perfectly Matched Layer (PML) with a width of 7.5µm was also introduced to prevent artificial reflections at the simulation boundaries. PMLs are crucial in ensuring accurate simulations by absorbing outgoing electromagnetic waves, preventing them from reflecting back and distorting the results. This allows for precise modeling of the fiber's optical properties and gas sensing performance without interference from boundary effects.

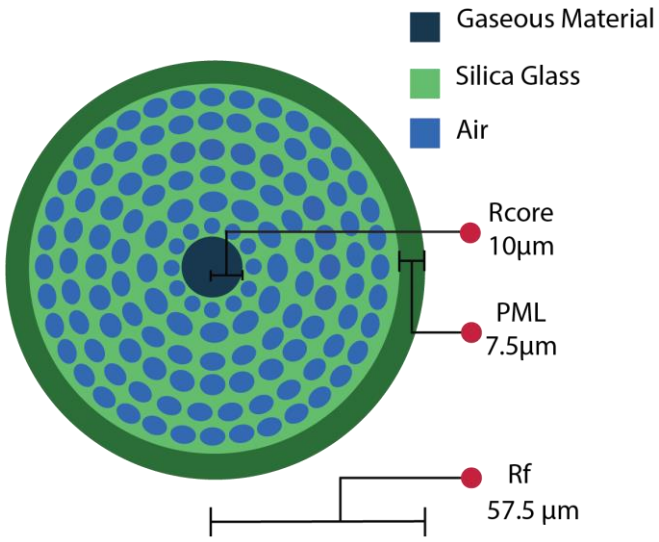

Figure 4.1: Basic structure of the proposed HC-PCF.

The structure comprises six layers of circular and elliptical holes, which can be seen from Figure 4.1. The starting layer around the hollow core is composed of circular holes with a radius of 2.5 µm, spaced 30 degrees apart. The second and fourth layers are composed of ellipses with a major axis length of 3.75 µm and a minor axis length of 2.5 µm. The ellipses of the second layer are arranged 30 degrees apart, while the ellipses of the fourth layer are positioned 15 degrees apart. The subsequent layers are constructed using ellipses with a major axis length of 3.75 µm and a minor axis length of 3.125 µm. Ellipses of the 3rd, 5th, and 6th layers have been set 20°, 12.5°, and 10° apart, respectively. The interlayer spacing between the first and second layers, third and fourth layers, and fifth and sixth layers is maintained at 2.5µm, while the spacing between the second and third layers and the fourth and fifth layers is set at 5µm.

4.2 Methodological Strategies for Optical Fiber Gas Sensing and Performance Analysis

During the design process of the hollow-core photonic crystal fiber (HC-PCF), several adjustments were made to optimize the confinement of light within the core, utilizing COMSOL Multiphysics for simulation. These modifications were crucial in identifying the appropriate modes that ensure effective light propagation and confinement in the fiber's core. Once the optimal design was achieved, simulations were conducted to extract the fiber's effective refractive index across a range of wavelengths. The wavelength spectrum was varied from 1000 nm to 2000 nm to analyze the fiber's optical response.

To accurately simulate the behavior of the silica-based fiber, the refractive index of silica was determined using Sellmeier's equation[75], a well-established method for defining the wavelength-dependent refractive index of transparent materials.

$$\eta_{silica} = \sqrt{1 + \frac{D_1\lambda^2}{\lambda^2 - K_1} + \frac{D_2\,\lambda^2}{\lambda^2 - K_2} + \frac{D_3\,\lambda^2}{\lambda^2 - K_3}} \tag{4.1}$$

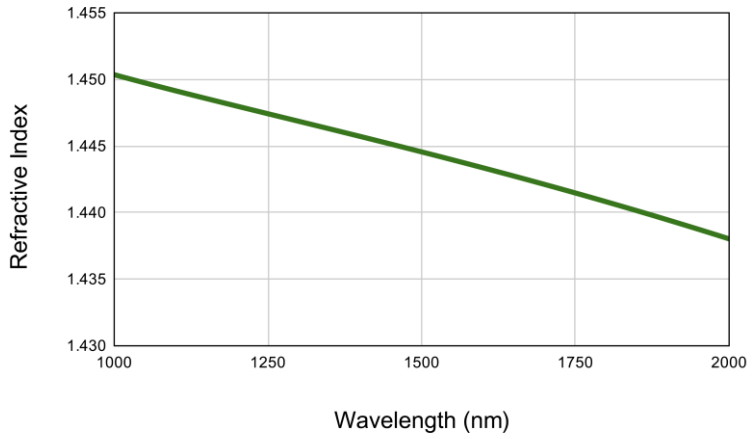

Figure 4.2: Refractive index of Silica as per Sellmeier's equation within the range of 1000 nm to 2000 nm.

The value of the constants (D_1, D_2, D_3, K_1, K_2, K_3) have been presented in Table.

Table 4.1: Constant values of sellmier's equation for silica

Constants	Values
D_1	0.696
D_2	0.40794
D_3	0.89748
K_1	0.004679 μm^2
K_2	0.013512 μm^2
K_3	97.934 μm^2

The gases selected for testing in this study include carbon dioxide (CO_2), methane (CH_4), and argon (Ar). These gases were specifically chosen to represent different categories of gaseous materials: CO_2 as an example of an inorganic gas, CH_4 as an organic gas, and argon as a noble gas. This diverse selection ensures that the sensing method is versatile across various types of gases.

The goal of this research is to develop a novel gas sensing technique utilizing ultra-short light pulses. By leveraging these pulses, the method aims to efficiently and accurately detect the type of gas present. This innovative approach could potentially enhance the sensitivity and selectivity of gas detection systems, providing a more effective solution for identifying a wide range of gases across different sectors.

The selected materials have their refractive index embedded into COMSOL from reliable source[76],[77],[78]. Those were implemented into the materials while running the simulations.

Initially, simulations were conducted using CO_2 as the test material to evaluate the performance of the designed hollow-core photonic crystal fiber (HC-PCF). The Figure 3.2 illustrates the COMSOL model of the fiber, showcasing its structural layout. To ensure the precision of the simulation results, a finer mesh size was employed (*Figure 3.3*). The use of a finer mesh is critical in computational simulations, as it allows for a more detailed representation of the physical model, leading to enhanced accuracy in the calculation of electromagnetic field distributions and other critical parameters. This ensures that the interaction between the gas and the optical fiber is modeled with the highest level of fidelity, ultimately improving the reliability of the results.

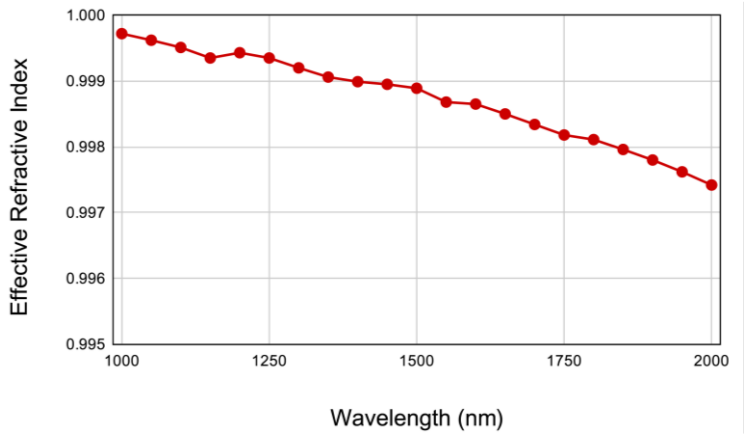

Figure 4.3: Effective Refractive index of HC-PCF filled with CO_2 vs wavelength.

Through COMSOL simulations, not only was the effective refractive index of the system calculated, but other important parameters such as the effective area and power fraction were also determined using the *equation 3.1* and *equation 3.2*.

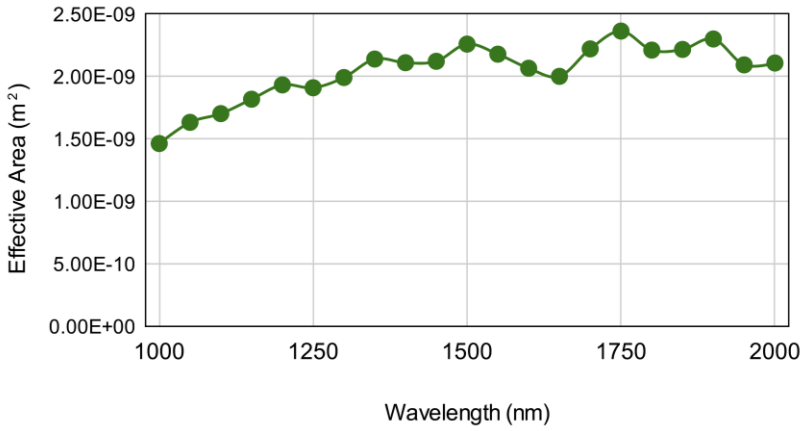

Figure 4.4: Effective Area of the HC-PCF filled with CO_2 vs wavelength.

These additional calculations provide a deeper understanding of the light-gas interaction within the HC-PCF. The effective area was determined to quantify the spatial extent of the optical mode within the fiber, while the power fraction was calculated to measure the power of light that is traveling through the core compared to the power of light that has been sent from one end.

After obtaining the desired data for the effective refractive index, effective area, and power fraction of the HC-PCF system filled with CO_2, several additional parameters were calculated. These key parameters include the dispersion parameter (D), nth-order dispersion term (β_n), and the nonlinear parameter (γ). The *equations 3.3-3.6* were used to extract these parameters.

Since the objective is to observe how ultra-short pulses evolve as they propagate through the HC-PCF filled with CO_2, the Nonlinear Schrödinger Equation (NLSE) needs to be solved. For this purpose, MATLAB was chosen, where the Split-Step Fourier Method (SSFM) is implemented to numerically solve the NLSE. In the code, the previously extracted parameters were provided as inputs to accurately model the system.

The ultra-short pulse that has been sent through the fiber has a Full Width at Half Maximum (FWHM) of 1 picosecond (ps) and a peak power of 1000 W, and follows a secant hyperbolic waveform. The shape of the input pulse for all the experiments presented in this manuscript also is of this type. However, these two parameters; pulse width and peak power; were carefully selected to ensure that the soliton number (N) remains greater than 1, a condition that is required for achieving the desired nonlinear effects during pulse propagation.

As the soliton number is connected with the mentioned parameters, they had to be adjusted to achieve the desired output. Additionally, the length of the system was set shorter than $L_{fission}$. $L_{fission}$ denotes the

length after which the pulse shape begins to distort, and its magnitude can be calculated using *equation 3.14*.

For the HC-PCF filled with CO_2, parameters have been extracted; such as- β_2 and β_3 from the effective refractive index graph, effective area at 1550 nm from effective area graph and nonlinear parameter (γ) by plugging the values in *equation 3.6*, where the value of n_2 has been chosen to match the same as silicas n_2. The extracted parameters have been shown in Table 4.2, and they have been used as input parameters to the SSFM code. These inputs enabled the analysis of the pulse shape using the SSFM method.

Table 4.2: Extracted input parameters for applying SSFM in HC-PCF filled with CO_2

Material in the core of HC PCF	**β_2 at 1550nm** (s^2/m)	**β_3 at 1550nm** (s^3/m)	**A_{eff} at 1550nm** **(m^2)**	**γ** **($W^{-1}m^{-1}$)**
CO_2	-1.31949×10^{-26}	7.26154×10^{-42}	2.18×10^{-9}	0.005758358

After the code was successfully run with the appropriate input parameters, the result at the output end was obtained, with the detailed analysis providing Compression Sensitivity and Power Increment [42],[43],[44]. For analyzing Compression Sensitivity the following equation has been used-

$$Compression\ Sensitivity = \frac{FWHM\ of\ compressed\ pulse}{FWHM\ of\ input\ pulse} \tag{4.2}$$

Compression Sensitivity is an important parameter used to quantify how much a pulse is compressed during its propagation through a medium or system. It specifically compares the Full Width at Half Maximum (FWHM) of the input pulse to the FWHM of the compressed pulse after the pulse has interacted with the system. This comparison provides a direct measure of how the pulse's duration has changed as a result of the system's effect.

The FWHM of the input pulse represents the width of the pulse at half of its maximum amplitude before any interaction or compression occurs. Typically measured in time (such as seconds or femtoseconds), the FWHM provides a clear representation of the duration over which the pulse maintains at least 50% of its maximum intensity. This measure of pulse width is critical because it defines the initial temporal characteristics of the pulse prior to compression.

After the pulse undergoes interaction or compression, the FWHM of the compressed pulse is determined through extrapolation of the curves. Compression typically occurs due to various physical effects, such as nonlinear optical interactions, that reduce the duration of the pulse. The FWHM of the compressed pulse, therefore, reflects how much the pulse has been shortened following this interaction. A reduced FWHM indicates that the pulse has been effectively compressed, leading to a shorter pulse duration.

This ratio provides a straightforward measure of how much the pulse has been compressed. A Compression Sensitivity value less than 1 signifies that the pulse has been shortened or compressed, meaning the duration of the pulse after compression is smaller than its initial duration. If the value is exactly 1, it indicates that no compression has occurred, and the pulse duration remains unchanged. A value greater than 1, though less common in compression studies, would indicate pulse broadening rather than compression.

For instance, if the input pulse has a FWHM of 100 femtoseconds (fs) and the compressed pulse is reduced to 20 fs, the resulting Compression Sensitivity would be calculated as 0.2. This value signifies that the pulse duration has been reduced to 20% of its original length, demonstrating effective compression.

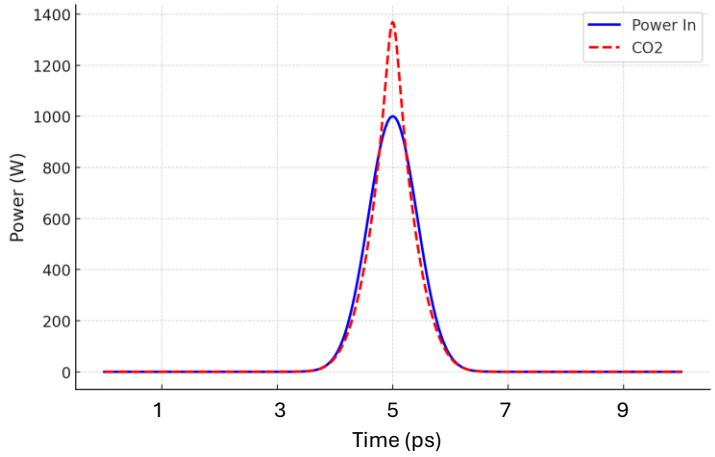

Figure 4.5: Comparison of the input pulse and the shape of pulse at the output.

From the *Figure 4.5*, it can be concluded that this proposed system, HC-PCF filled with CO_2, has been successful in compressing the input pulse, and the Compression sensitivity has been an impressive amount of 64% and the power upsurge has been noticed of 369.07 W.

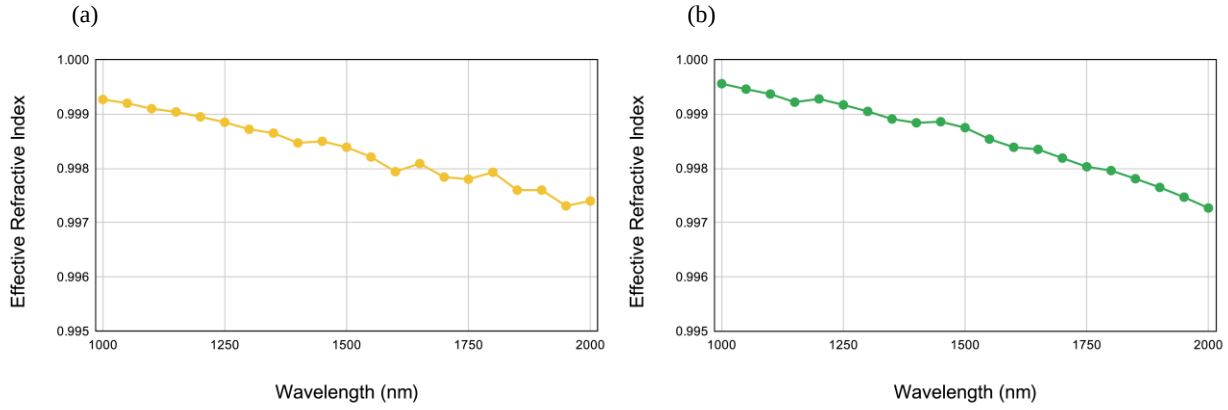

Figure 4.6: a) Effective Refractive index of HC-PCF filled with CH_4 vs wavelength, b) Effective Refractive index of HC-PCF filled with Ar vs wavelength.

The same procedure was repeated for systems where the HC-PCF was filled with CH_4 (methane) and Ar (Argon). By following the identical steps of parameter extraction and pulse propagation analysis, highly precise and satisfactory results have been observed. These findings were consistent across both gas-filled configurations, confirming the robustness and accuracy of the simulation process.

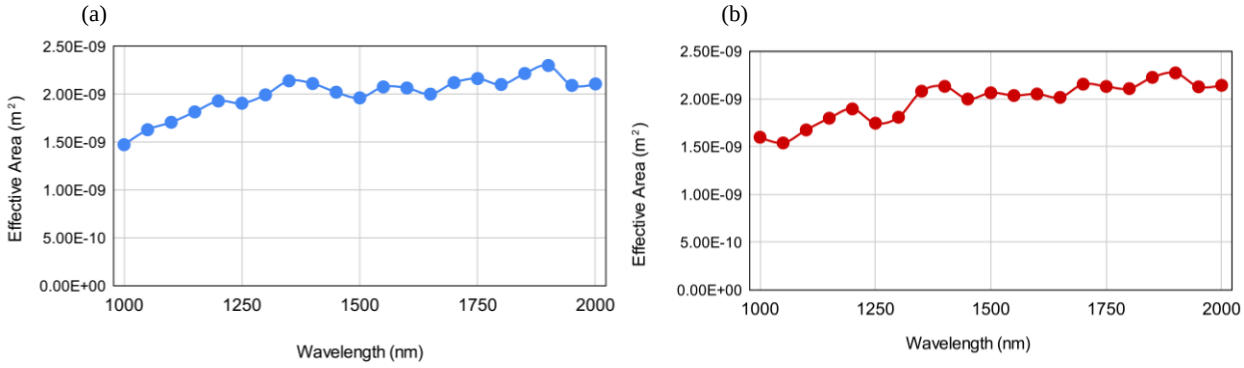

Figure 4.7: a) Effective Area of HC-PCF filled with CH_4 vs wavelength , b) Effective Area of HC-PCF filled with Ar vs wavelength.

Using these information, other important input parameters for SSFM have been calculated and demonstrated in Table 4.3

Table 4.3: Extracted input parameters for applying SSFM in HC-PCF filled with gaseous materials

Material in the core of HC PCF	**β_2 at 1550nm** (s^2/m)	**$\beta_3$at 1550nm** (s^3/m)	**A_{eff} at 1550nm** (m^2)	**γ** ($W^{-1}m^{-1}$)
CO_2	-1.31949×10^{-26}	7.26154×10^{-42}	2.18×10^{-9}	0.005758358
CH_4	-1.19754×10^{-26}	-1.28051×10^{-41}	2.1779×10^{-9}	0.005747685
Ar	8.43012×10^{-27}	-3.51072×10^{-41}	2.04×10^{-9}	0.005124

Utilizing these input parameters SSFM has been applied for the HC-PCF system, the length of the system has been chosen 1 meter as the Fission length and the soliton Number (Table 4.4) for these cases allowed to have a length of 1m.

Table 4.4: Soliton Number and Fission Length for the test cases

Material in the core of HC PCF	**Soliton Number (N)**	**$L_{fission}$**
CO_2	12.5460	2.1787 m
CH_4	13.1571	2.2891 m
Ar	14.8062	2.8896 m

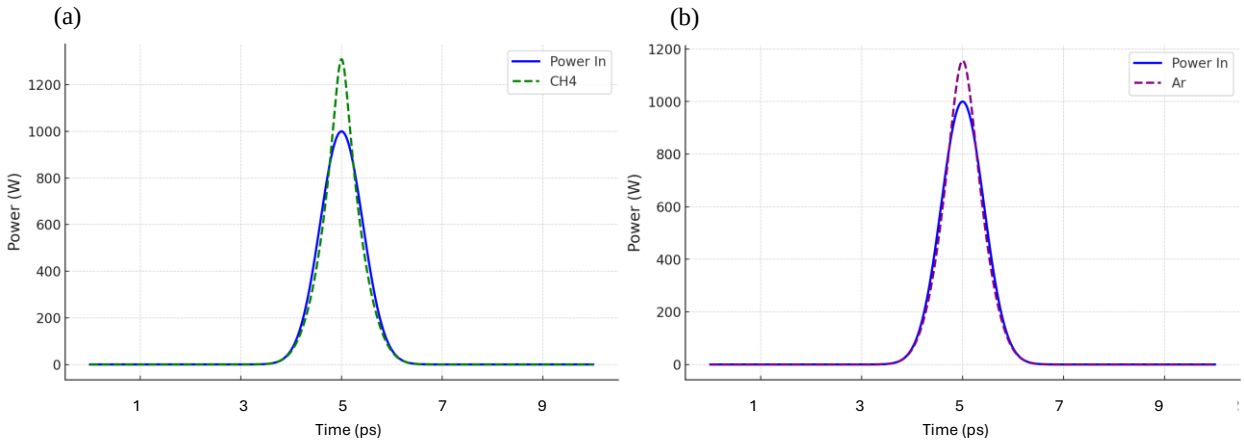

Figure 4.8 a) *Comparison of the input pulse and the shape of pulse at the output for CH_4, b) Comparison of the input pulse and the shape of pulse at the output for Ar.*

Table 4.5: Information of the pulse as it propagates through different core materials of HC-PCF.

Material in the core of HC PCF	**Power of the input pulse**	**Power of the output pulse**	**Compression Sensitivity**
CO_2	1000 W	1369.07 W	64%
CH_4	1000 W	1309.7 W	68%
Ar	1000 W	1155.65 W	82%

The findings (*Figure 4.5* and *Figure 4.8*) indicate that gas sensing can be effectively conducted using ultrashort pulses in Hollow-Core Photonic Crystal Fibers (HC-PCF). As it can be observed from the experiments that a maximum power increase of 369.07 W and a minimum compression sensitivity of 64% has been recorded. This demonstrates the potential of the proposed method for reliable gas detection.

Unlike traditional sensing methods that utilize optical fibers, this approach requires fewer analyzing devices, as this method relies only on just two parameters for detection: pulse compression and power upsurge.

In contrast, existing methods typically rely on analyzing multiple detection parameters such as relative sensitivity, numerical aperture, effective area, effective material loss (EML), and confinement loss. These parameters not only increase the complexity of the experiment but also require additional devices to measure each one, making the setup more complicated. The proposed method, by focusing on just two key parameters, offers a more streamlined and efficient approach to gas sensing.

4.3 Proposed Experimental Setup

The proposed novel sensing technique has been verified through simulations and codes. However, for practical implementation, a mode-locked ultra-fast laser centered at a 1550 nm wavelength, facilitated by IPG Photonics, will be used as the source. The laser source is tunable across a wide power range, up to 3KW. For the experiments represented in this manuscript, input powers were varied between 300W and 1000W for different setups.

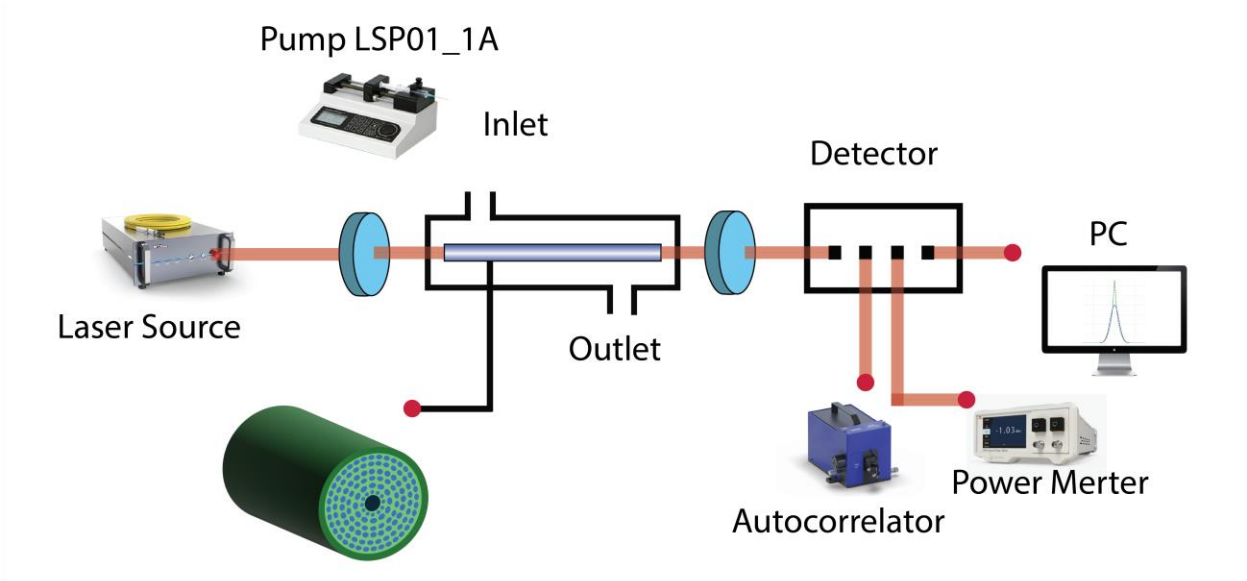

Figure 4.9: Proposed experimental setup.

This offers Ytterbium and Erbium continuous waves of 1-3 picoseconds at a repetition rate of 200KHz which can provide a variety of polarization and linewidth options [79]. A coupling system of the lens (fused silica plan convex lens with 50nm focal length) along with a beam expander will be utilized to focus the laser beam to the fiber [80]. A programmable micro injection pumper, specifically the LSP01-1A model manufactured by LongerPump™, will be employed to inject the analyte into the channel. The refuse reservoir is connected to the channel's outlet to store the used analyte [81]. The compression of an input pulse of a specific watt will be induced by the presence of unknown analytes, and this compression can be detected using a power meter. The variable delay will be adjusted by the autocorrelator as the pulse is delayed from input to output. A dedicated PC facilitated as HMI (human to machine interface) will be connected to have automated control of pulses. *Figure 4.9* incorporates the experimental setup starting from laser source up to detectors.

Chapter 5

HC-PCF as Refractive Index Sensor and its Performance Analysis

Using the same basic principles stated in previous chapters, we explored hollow-core photonic crystal fibers (HC-PCFs) for materials with refractive indices in the range of 1.4 to 1.45. This range was selected because many common liquids, few organic and inorganic solvents, have refractive indices that fall within this range. Accurately detecting the refractive index of liquids in this range is important for various applications, including chemical sensing, environmental monitoring, and medical diagnostics. The materials that were examined, along with their refractive indices, are listed in the table below.

Table 5.1: List of materials having refractive index within 1.4 -1.45

Name of the material	Refractive Index
Ethylene tetrafluoroethylene (ETFE)	1.403 [82]
Sylgard 184 (polydimethylsiloxane)	1.4118 [83]
Sugar solution, 50%	1.42 [84]
Hexanol	1.414 [85]
Ethylene glycol	1.431 [85]
Choloform	1.4459 [85]

To evaluate the newly developed sensing method for liquid materials, detailed simulations were conducted. The objective was to assess the capability of the HC-PCF to detect small variations in refractive index when filled with different liquids. The results were highly promising, demonstrating that the method operates efficiently and accurately in sensing even minor changes in refractive index. These findings suggest that the technique holds potential for a broad range of practical applications.

Additionally, the simulations showed that the light confinement and guiding properties of the HC-PCF work well for detecting refractive indices within this range. By adjusting the fiber's design and optimizing the core structure, we improved the system's sensitivity and accuracy. This makes it a strong option for advanced sensing applications in fields such as pharmaceuticals, food safety, and environmental science, where precise liquid sensing is needed.

In summary, the proposed sensing technique, verified through simulations, has proven to be an efficient and reliable way to detect refractive index changes in liquids. This advancement could lead to new opportunities for using HC-PCFs in a wide variety of industries.

5.1 Design and Simulation

An HC-PCF was developed to detect materials with refractive indices ranging from 1.4 to 1.45. The fiber, primarily made of silica glass, includes air-filled cavities that surround its core, facilitating effective light transmission within the core region. Samples are introduced into the core, where ultra-short laser pulses are transmitted. The sensing mechanism is based on observing and analyzing changes in the pulse shape. This innovative method utilizes the distinct properties of HC-PCF in combination with ultra-short pulse lasers, providing a highly sensitive and precise approach for detecting materials with refractive indices in this range. This technique is particularly useful for maintaining quality control in industries where such materials are used.

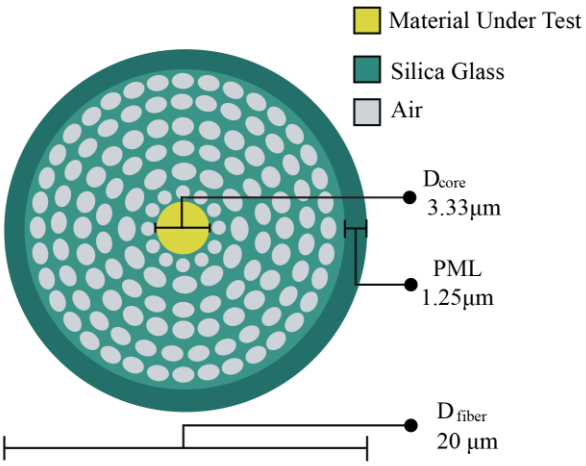

Figure 5.1: Basic structure of the proposed HC-PCF for refractive index sensing.

The fiber design was completed using COMSOL Multiphysics software, and its functionality was confirmed through simulations that demonstrated successful light confinement within the core. As depicted in *Figure 5.1*, the fiber has an overall diameter of 20µm and a core diameter of 3.33µm. The air holes are arranged in six layers surrounding the core. The first layer consists of circular air holes with a diameter of 0.83µm, spaced 30° apart in a circular pattern. The next five layers contain elliptical air holes in two configurations: one type with a major axis of 0.625µm and a minor axis of 0.42µm, and another with a major axis of 0.625µm and a minor axis of 0.52µm. The second and fourth layers include the first type of elliptical holes, spaced 30° and 15° apart, respectively. The second type is placed in the third, fifth,

and sixth layers, with spacing of 20°, 12.5°, and 10°, respectively. In addition, a perfectly matched layer 1.25μm wide was added to prevent light wave reflections back into the system[43],[44].

The fiber and core diameters have been selected within this range to ensure the fiber functions in a single mode, considering the V number $\cong 2.405$ or less than the exact value.

$$V = \frac{2\pi}{\lambda} r \sqrt{{n_{core}}^2 - {n_{cladding}}^2} \tag{5.1}$$

Where, *r* is the radius of the core.

The dimensions and orientation of the air holes were meticulously determined through a process of trial and error, with the values being firmly established following the observation of satisfactory output.

5.2 Methodological Strategies for Refractive Index Sensing and Performance Analysis

Once the HC-PCF was meticulously designed for optimal performance, simulations were conducted to determine the effective refractive index of the entire system across wavelengths ranging from 1300 nm to 2000 nm. During this process, the refractive index of silica glass was set according to Sellmeier's equation[75] (*Equation 4.1*).

The testing materials are chosen to have refractive indices of 1.4,1.425,1.45 respectively. Those were implemented into the materials under test (MUT) while running the simulations in COMSOL.

Initially, simulations were conducted using material with refractive index of 1.4 as the test material to evaluate the performance of the designed HC-PCF. To ensure the precision of the simulation results, a finer mesh size was also employed here.

For this case, not only the effective refractive index of the system was calculated but also other important parameters such as the effective area and power fraction in COMSOL, using the *equation 3.1* and *equation 3.2*.

After obtaining the desired data for the effective refractive index, effective area, and power fraction of the hollow-core photonic crystal fiber (HC-PCF) system filled with material with refractive index of 1.4; several additional parameters were calculated like the previous case. These key parameters include the dispersion parameter (D), n^{th}-order dispersion term (β_n), and the nonlinear parameter (γ). The *equations 3.3-3.6* were used to extract these parameters.

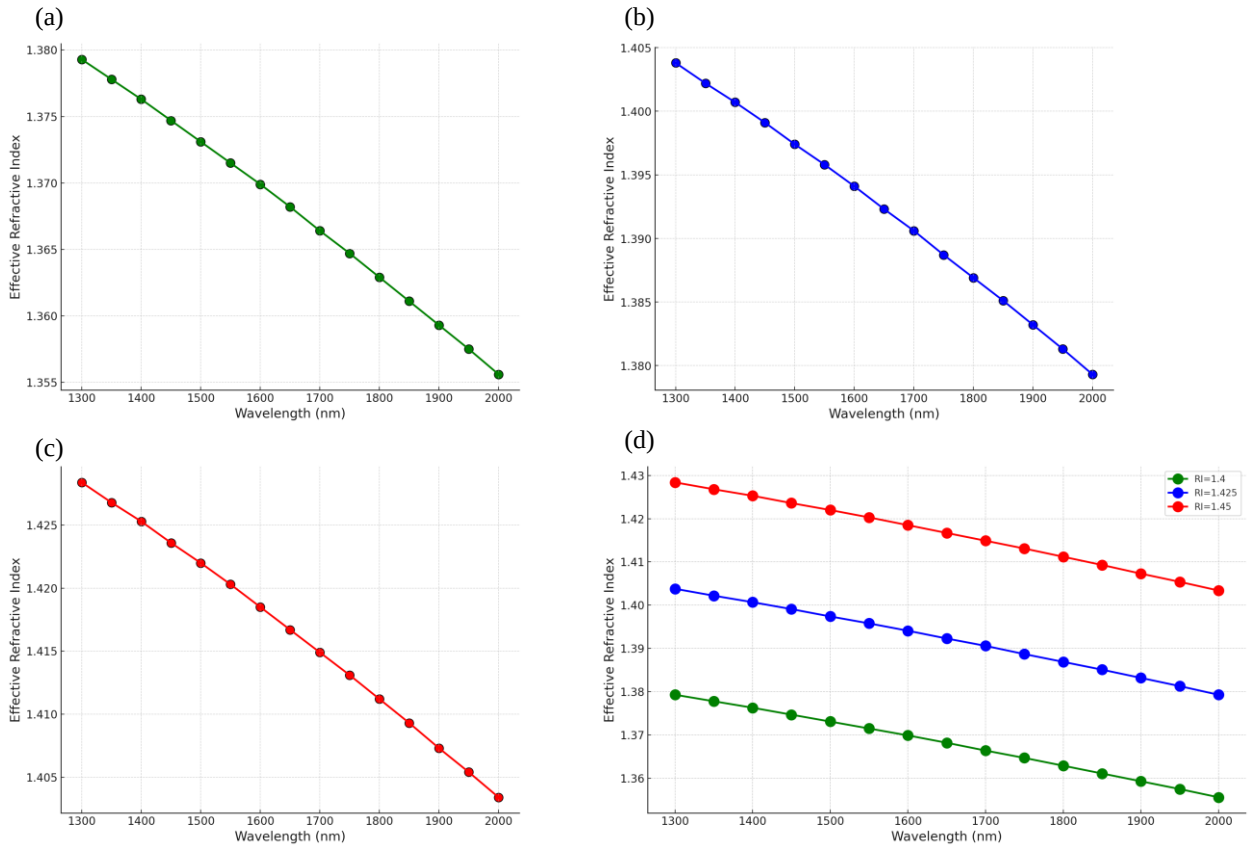

Figure 5.2: a) Effective Refractive Index vs Wavelength for MUT with refractive index of 1.4, b) Effective Refractive Index vs Wavelength for MUT with refractive index of 1.425, c) Effective Refractive Index vs Wavelength for MUT with refractive index of 1.45, d) Comparison of Effective Refractive Indices of the MUT's.

Table 5.2: Extracted input parameters for applying SSFM in HC-PCF filled with materials with varying refractive indices

Refractive index of MUT	$\boldsymbol{\beta_2}$ **at 1550 nm** (s^2/m)	$\boldsymbol{\beta_3}$ **at 1550 nm** (s^3/m)	$\boldsymbol{A_{eff}}$ **at 1550 nm** (m^2)	$\boldsymbol{\gamma}$ ($W^{-1}m^{-1}$)
1.4	-1.00816×10^{-25}	-6.0427×10^{-41}	8.1432×10^{-12}	0.0149335
1.425	-1.08139×10^{-25}	-3.72209×10^{-40}	7.9789×10^{-12}	0.015241
1.45	-1.06191×10^{-25}	3.63436×10^{-41}	7.8252×10^{-12}	0.01554

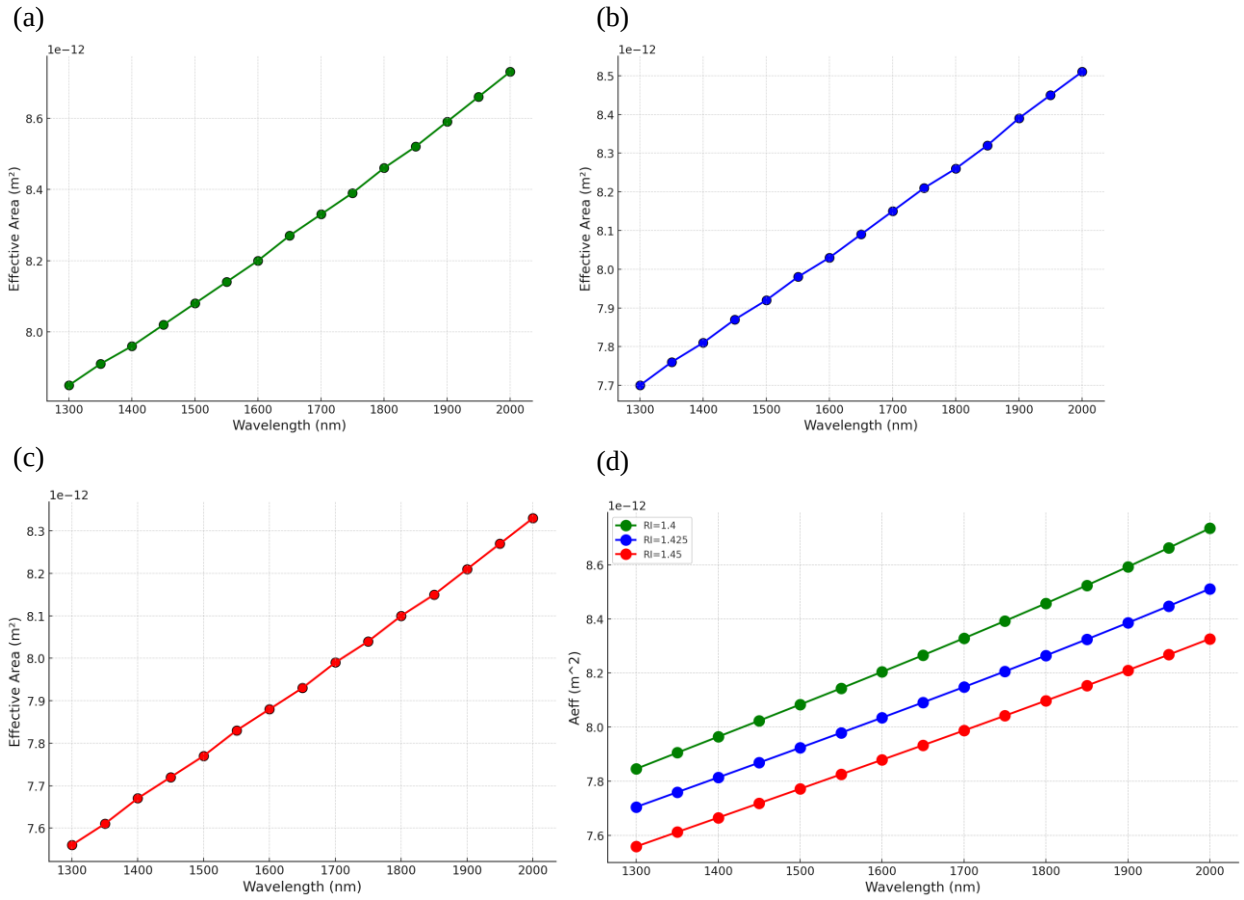

Figure 5.3: a) Effective Area vs Wavelength for MUT with refractive index of 1.4, b) Effective Area vs Wavelength for MUT with refractive index of 1.425, c) Effective Area vs Wavelength for MUT with refractive index of 1.45, d) Comparison of Effective Area of the MUT's.

Using the extracted information, simulations have been conducted with the NLSE code to analyze how an ultrashort pulse propagates through an HC-PCF. In the test case, the pulse source power was set to 1000 W, and a pulse duration with a Full Width at Half Maximum (FWHM) of 1 picosecond was selected.

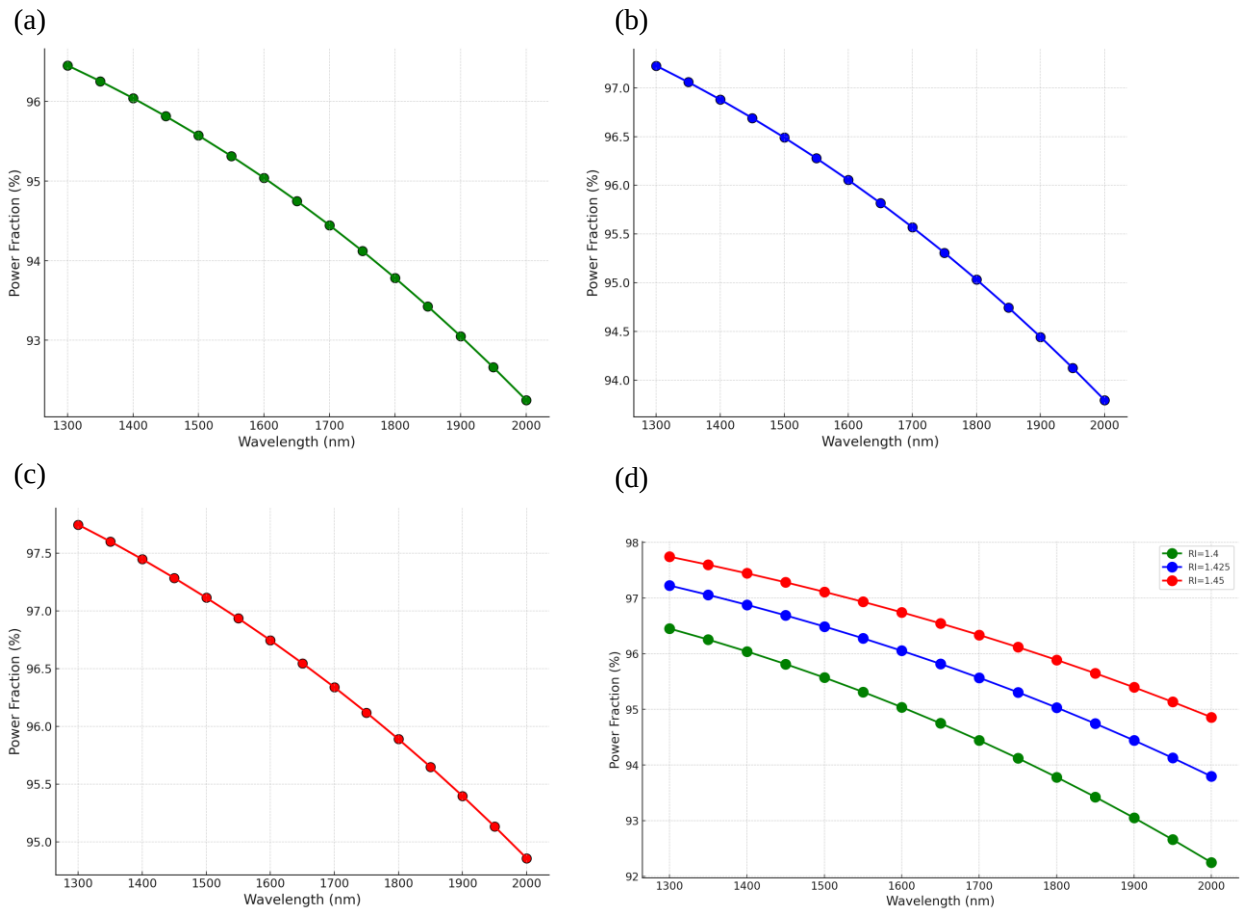

Figure 5.4: a) Power Fraction vs Wavelength for MUT with refractive index of 1.4, b) Power Fraction vs Wavelength for MUT with refractive index of 1.425, c) Power Fraction vs Wavelength for MUT with refractive index of 1.45, d) Comparison of Power Fraction of the MUT's.

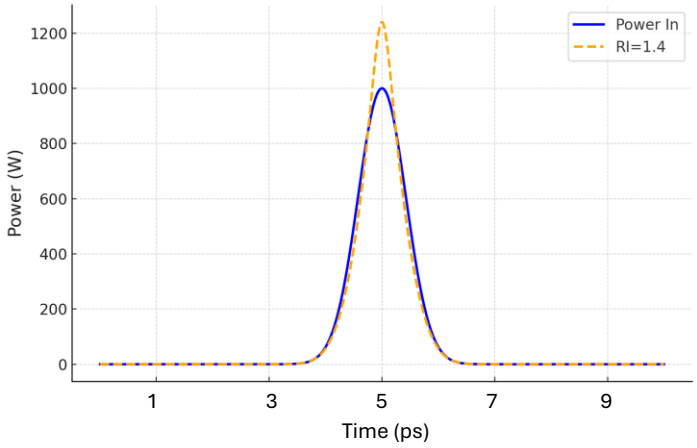

Figure 5.5: Comparison of the input pulse and the shape of pulse at the output for MUT with RI of 1.4, when the length of HC-PCF is 0.2m.

Important parameters such as the fission length ($L_{fission}$) and the soliton number (N) were analyzed. The fission length refers to the distance over which a higher-order soliton splits into fundamental solitons due to perturbations, while the soliton number indicates the order of the soliton based on the pulse and fiber properties.

By adjusting the fiber length within the range of $L_{fission}$ the effects on the output pulse were observed. It was found that as the fiber length approached $L_{fission}$, higher compression of pulses and an increase in power occurred. This increased sensitivity enables a more effective distinction of the material properties.

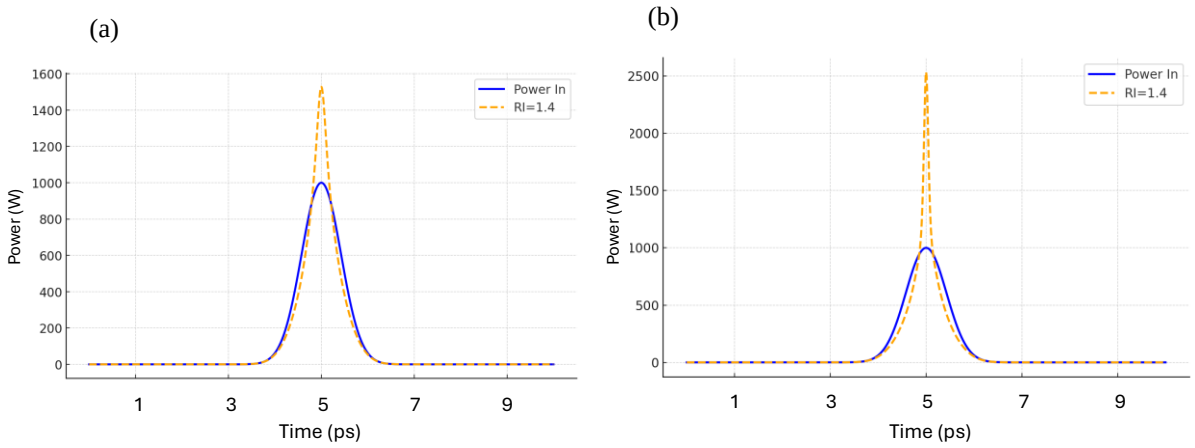

Figure 5.6: Comparison of the input pulse and the shape of pulse at the output for MUT with RI of 1.4, when the length of HC-PCF is- a) 0.25m, b)0.3m

Table 5.3: Information of the pulse as it propagates through HC-PCF filled with MUT having RI of 1.4

Refractive index of MUT	Soliton Number	Fission Length	Length of the HC-PCF	Compression Sensitivity	Power Upsurge
1.4	7.3093	0.4894	0.2 m	74.3%	240.7 W
			0.25 m	52.2%	528.302 W
			0.3 m	17.98%	1535.322 W

The same process was repeated for HC-PCFs with core materials having refractive indices of 1.425 and 1.45. These fibers were also tested with different lengths (0.2m,0.25m and 0.3m) to examine how these factors influence the pulse propagation.

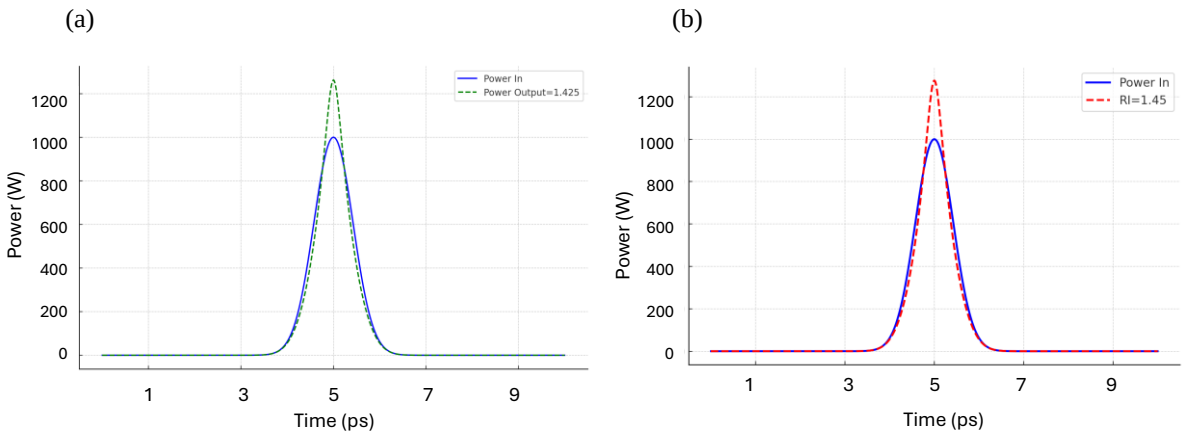

Figure 5.7: Comparison of the input pulse and the shape of pulse at the output for MUT with RI of- a) 1.425,b)1.45; when the length of HC-PCF is 0.2m.

Table 5.4: Information of the pulse as it propagates through HC-PCF filled with MUT having varying RI when length of the HC-PCF was set to 0.2m

Refractive index of MUT	Soliton Number	Fission Length	Length of the HC-PCF	Compression Sensitivity	Power Upsurge
1.4	7.3093	0.4894	0.2	74.3%	240.7 W
1.425	7.1297	.4678	0.2	70.6%	262.743 W
1.45	7.2651	0.46748	0.2	69.8%	276.62 W

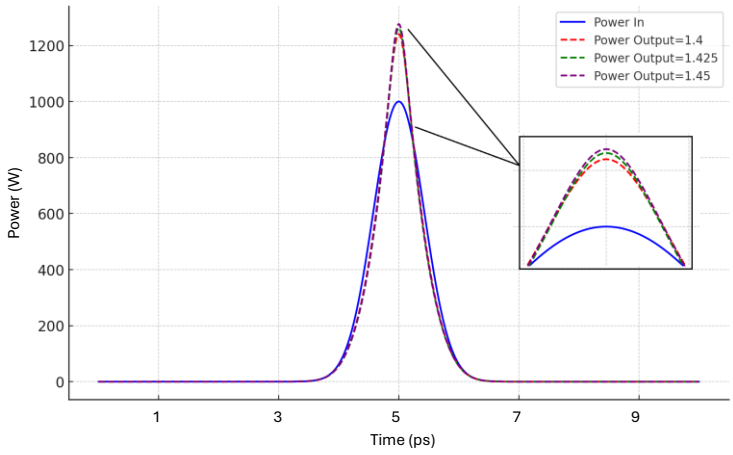

Figure 5.8: Comparison of the input pulse and the shape of pulses at the output for MUT with varying RI when the length of HC-PCF is 0.2m.

From the *Table 5.4* and *Figure 5.8*, it is evident that our system is well capable of showing unique results for materials of different refractive indices. For the HC-PCF length of 0.2m, minimum compression sensitivity of 69.8% and maximum power upsurge of 276.62 W have been observed.

Results were different when the length of HC-PCF was set 0.25m.

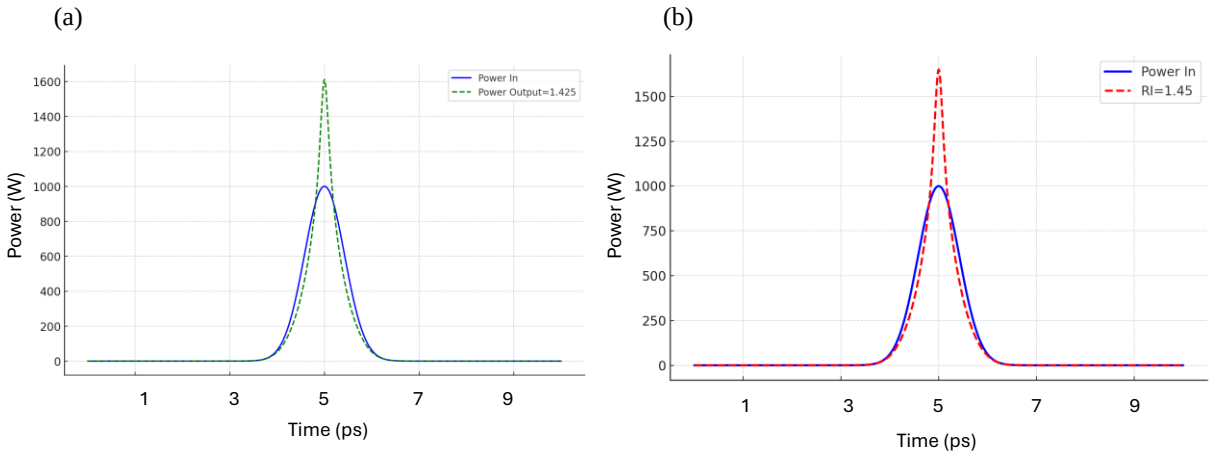

Figure 5.9: Comparison of the input pulse and the shape of pulse at the output for MUT with RI of- a) 1.425,b)1.45; when the length of HC-PCF is 0.25m.

Table 5.5: Information of the pulse as it propagates through HC-PCF filled with MUT having varying RI when length of the HC-PCF was set to 0.25m

Refractive index of MUT	**Soliton Number**	**Fission Length**	**Length of the HC-PCF**	**Compression Sensitivity**	**Power Upsurge**
1.4	7.3093	0.4894	0.25	52.2%	528.302 W
1.425	7.1297	0.4678	0.25	45.8%	611.4 W
1.45	7.2651	0.46748	0.25	44.9%	650.58 W

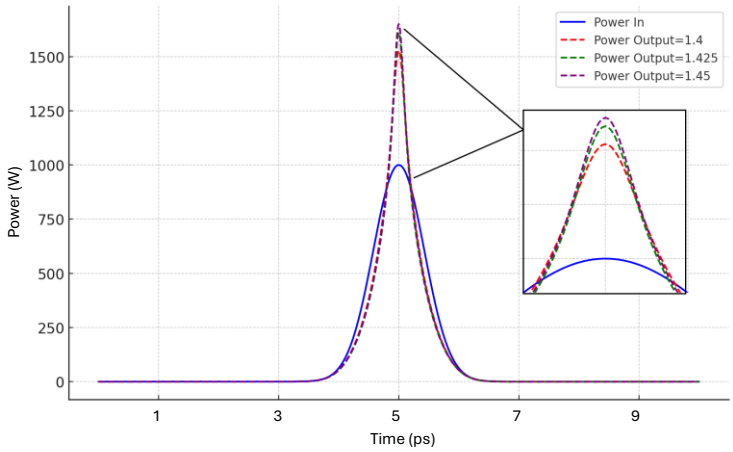

Figure 5.10: Comparison of the input pulse and the shape of pulses at the output for MUT with varying RI when the length of HC-PCF is 0.25m.

From *Figure 5.10* and *Table 5.5*, it is evident that the developed system works more efficiently if the length is chosen closer to the fission length. From the analysis done, the minimum compression sensitivity achieved is 44.9% and maximum power upsurge achieved is 650.58 W.

Another analysis was conducted with the HC-PCF length set to 0.3 m, and this adjustment led to further improvements in the results.

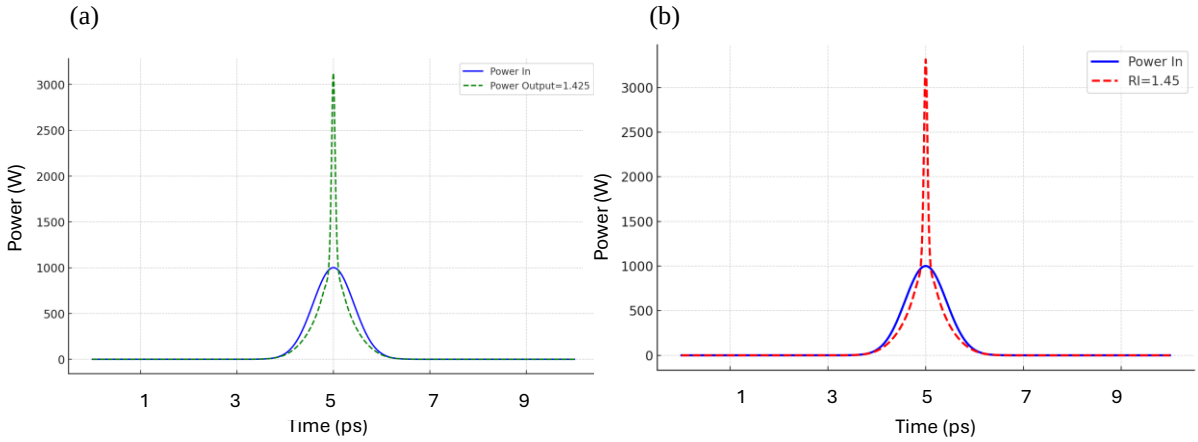

Figure 5.11: Comparison of the input pulse and the shape of pulse at the output for MUT with RI of- a) 1.425, b)1.45; when the length of HC-PCF is 0.3m.

Table 5.6 Information of the pulse as it propagates through HC-PCF filled with MUT having varying RI when length of the HC-PCF was set to 0.3m

Refractive index of MUT	Soliton Number	Fission Length	Length of the HC-PCF	Compression Sensitivity	Power Upsurge
1.4	7.3093	0.4894	0.3	17.98%	1535.322 W
1.425	7.1297	.4678	0.3	14.2%	2158.856 W
1.45	7.2651	0.46748	0.3	11.6%	2313.918W

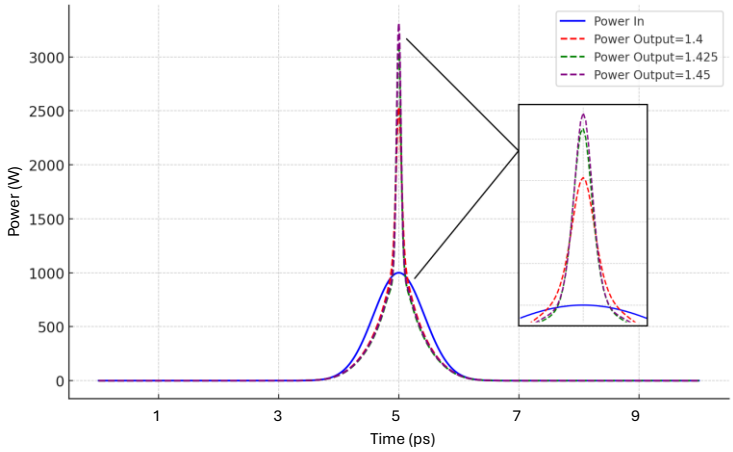

Figure 5.12: Comparison of the input pulse and the shape of pulses at the output for MUT with varying RI when the length of HC-PCF is 0.3m.

From this case, the minimum compression sensitivity achieved is 11.6% and maximum power upsurge achieved is 231.918 W.

An overall comparison of the achieved results has been demonstrated in the table below.

Table 5.7: Overall comparison of the achieved results

Refractive index of MUT	Length of the HC-PCF= 0.2m		Length of the HC-PCF= 0.25 m		Length of the HC-PCF= 0.3 m	
	Compression Sensitivity	Power Upsurge	Compression Sensitivity	Power Upsurge	Compression Sensitivity	Power Upsurge
1.4	74.3%	240.7 W	52.2%	528.302 W	17.98%	1535.322 W
1.425	69.8%	262.743 W	45.8%	611.4 W	14.2%	2158.856 W
1.45	70.6%	276.62 W	44.9%	650.58 W	11.6%	2313.918W

Findings from the experiment indicate that this HC-PCF system is equally effective, efficient and reliable as refractive index sensor. Distinct value of pulse compression sensitivity and power uprise is seen for each cases.

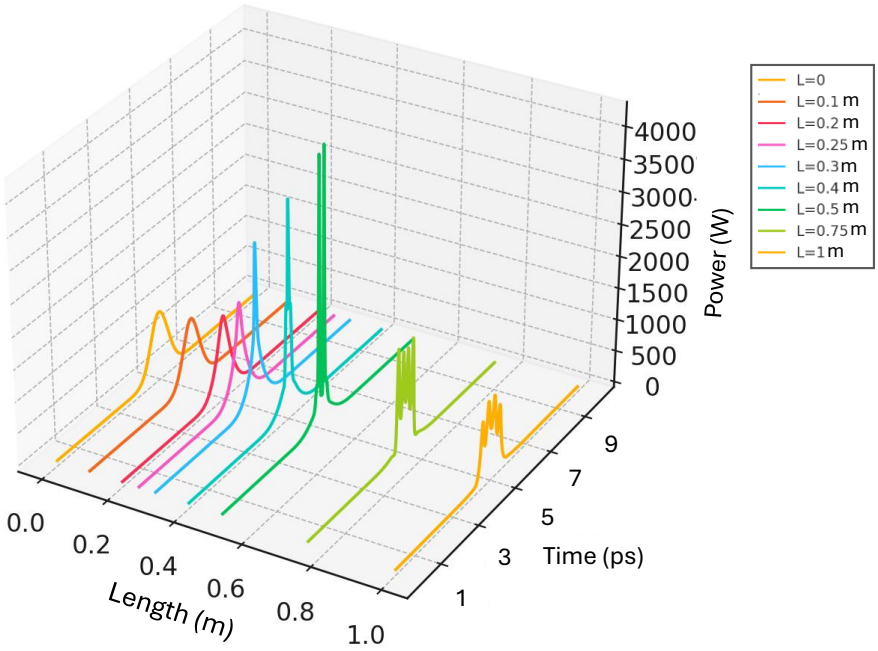

Figure 5.13: Shape of the pulse as it propagated through HC-PCF filled with MUT having RI 1.4.

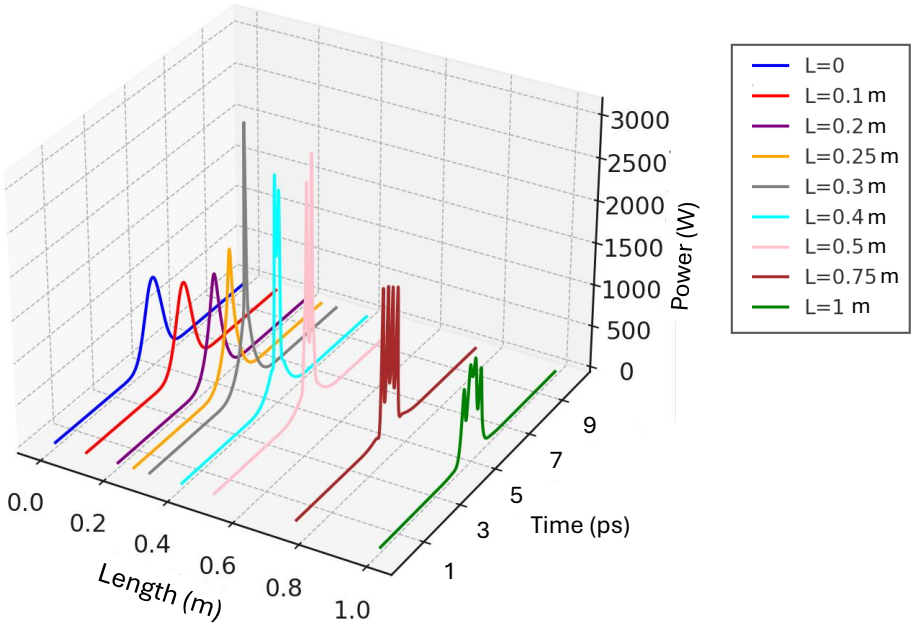

Figure 5.14: Shape of the pulse as it propagated through HC-PCF filled with MUT having RI 1.425.

It was also observed that pulse compression became more pronounced as the system length approached the fission length. A detailed analysis was conducted to investigate this phenomenon. The HC-PCF, filled with a MUT having RI of 1.4 and 1.425, was tested with varying fiber lengths. The results, as shown in the *Figure 5.13* and *Figure 5.14*, indicate that pulse distortion began when the fiber length was set to 0.4 m, even though the pulse was expected to maintain its shape before reaching the fission length. This unexpected distortion occurred due to the loss coefficient as specified in *equation 3.7* which was set to 0.22 dB/km , for all the experiments presented in this manuscript.

Beyond this length, it became evident that the pulse shape degraded significantly as it propagated further, eventually becoming entirely distorted. This demonstrates that the chosen system parameters, particularly the loss coefficient, play a crucial role in pulse behavior, especially when operating near or beyond the fission length. Understanding these effects is essential for optimizing system performance and achieving the desired pulse characteristics in practical applications.

A vital take away from the analysis is that the length of the HC-PCF should be kept closer to the value of fission length. The most efficient result has been achieved when we set the length of our device closer to that.

5.3 Applications of Refractive Index Sensing Using HC-PCF

After closely analyzing the results obtained from materials with refractive indices of 1.4, 1.425, and 1.45 in the core of hollow-core photonic crystal fibers (HC-PCF), we observed encouraging outcomes that suggest significant potential in various applications. The performance of the HC-PCFs with these refractive indices demonstrated clear trends, especially in terms of light transmission, confinement, pulse compression and efficiency. Given that many materials commonly used in photonic applications exhibit refractive indices in this range, it became evident that this discovery could open doors for broader practical implementations.

With the initial results in hand, the investigation is set to be expanded by testing additional configurations and exploring the broader potential of these refractive index values in real-world applications.

5.3.1 Sensing pure solvents through pulse compression using HC-PCF

Chemicals such as acetone, ethanol, hexane, isopropanol, and hexanol play a vital role in various industries and medical applications, making their purity and quality crucial. Ensuring these substances are free from contamination is essential to maintaining their effectiveness and suitability for diverse applications[86]-[89]. The novel detection method presented in this manuscript, which utilizes ultra-short pulses transmitted through an HC-PCF for sensing, has been applied to detect these materials. This method has enabled us to achieve remarkable sensitivity in pulse compression and power amplification, with results customized to each specific input configuration.

Table 5.8: Refractive Index of the sample pure solvents

Core-filling substances	Effective Refractive index
Acetone	1.3589
Ethanol	1.3614
Hexane	1.375
Isopropanol	1.3772
Hexanol	1.4140

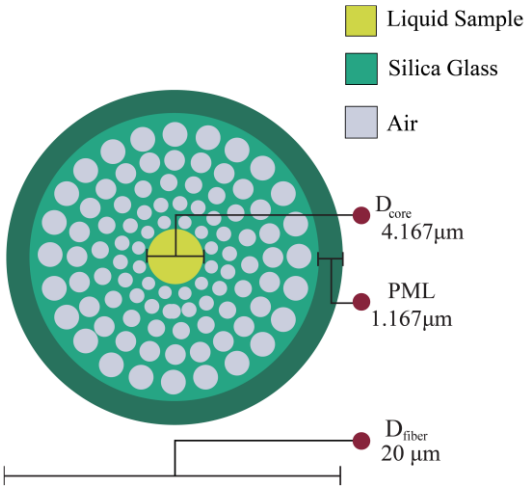

Figure 5.15: HC-PCF designed to detect pure solvents.

A uniquely designed HC-PCF (*Figure 5.15*) has been used specifically for detecting materials with refractive indices between 1.4 and 1.45, was utilized in this study. The core has a diameter of 4.1667 µm. Surrounding the core is the first layer, consisting of 12 air holes, each with a diameter of 0.8333 µm, and spaced 30° apart. The second layer contains 18 air holes, each separated by 20° and measuring 1.042 µm in diameter. The third, fourth, and fifth layers contain 18, 24, and 24 air holes, respectively. The air holes

in the third layer have a diameter of 1.25 µm, while those in the fourth layer are 1.458275 µm in diameter, and the fifth layer's air holes measure 1.666 µm. The remainder of the photonic crystal fiber is composed of fused silica, with a diameter of 20 µm, and is surrounded by a perfectly matched layer that has a width of 1.6667 µm.

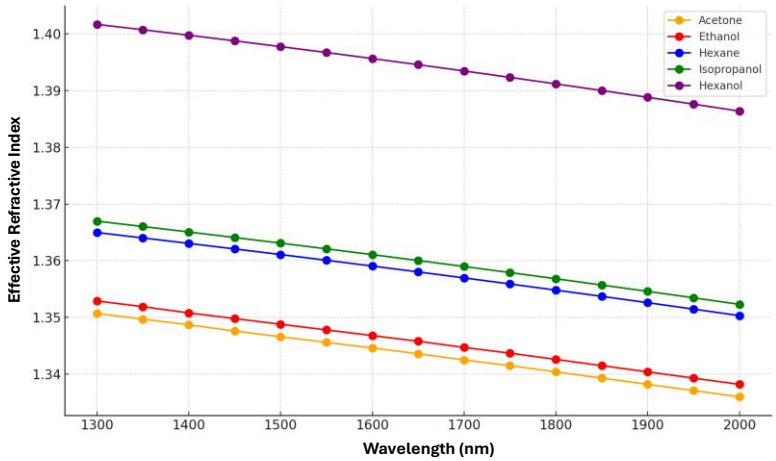

Figure 5.16: Comparison of Effective Refractive Indices of the sample pure solvents.

Silica was selected as the base material, and the Sellmeier equation was applied accordingly. The materials chosen for testing include Acetone, Ethanol, Hexane, Isopropanol, and Hexanol, with their respective refractive indices provided in the table below. Using COMSOL Multiphysics, the refractive index for each material was assigned based on the *Table 5.8*. Simulations were then conducted to determine the Effective Refractive Index, Effective Area, and Power Fraction for each case.

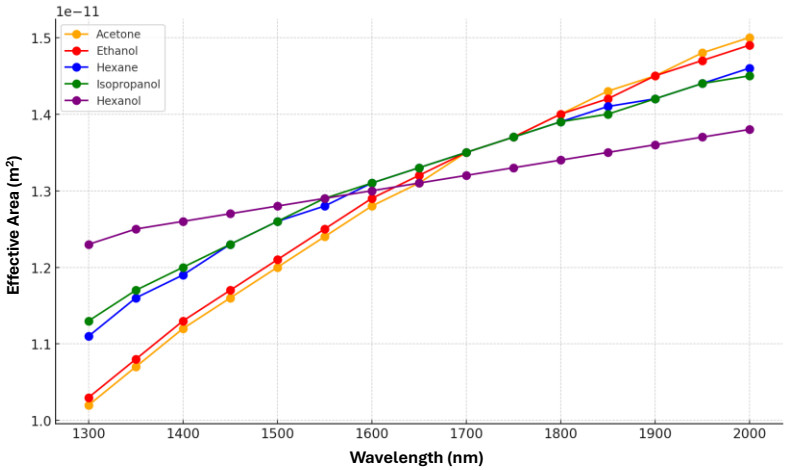

Figure 5.17: Comparison of Effective Area of the sample pure solvents.

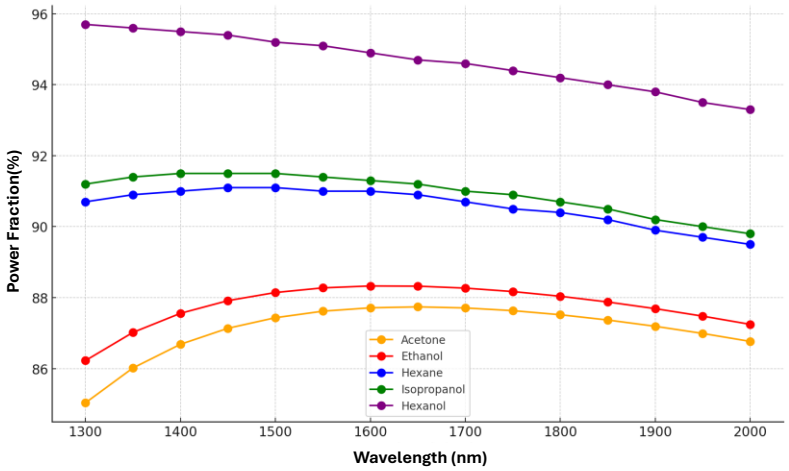

Figure 5.18: Comparison of Power Fraction of the sample pure solvents.

From the data extracted through COMSOL Simulations, a few important parameters for sensing were also calculated. They are given in Table 5.9.

Table 5.9: *Extracted input parameters for applying SSFM in HC-PCF filled with sample pure solvents*

Name of Pure solvent	**Refractive Index**	**β_2 at 1550 nm** (s^2/m)	**β_3 at 1550 nm** (s^3/m)	**A_{eff} at 1550 nm** (m^2)	**γ** ($W^{-1}m^{-1}$)
Acetone	1.3589	-1.3536×10^{-26}	7.102×10^{-40}	1.244×10^{-11}	0.0097741
Ethanol	1.3614	-3.1116×10^{-26}	5.667×10^{-40}	1.251×10^{-11}	0.0097187
Hexane	1.375	-4.459×10^{-26}	1.2557×10^{-40}	1.282×10^{-11}	0.0094840
Isopropanol	1.3772	-4.644×10^{-26}	1.229×10^{-40}	1.285×10^{-11}	0.0094272
Hexanol	1.4140	-6.3325×10^{-25}	1.213×10^{-40}	1.290×10^{-11}	0.0094463

With these important parameters being extracted, the code on MATLAB was run where NLSE is solved using SSFM, to observe the changes in ultra short pusles sent through our designed HC-PCF. Unique responses have been recorded for each test materials.

The input pulse width was varied as 1ps and 2ps while exploring the input power levels in 600W and 700W. A comprehensive analysis has been conducted to understand how solvent characteristics impact pulse compression.

As previously mentioned, the fiber length was carefully adjusted to meet the conditions of fission length ($L_{fission} > L$) and soliton number ($N > 1$) across different refractive indices. Although the pulse width and input power varied, the central wavelength was maintained at 1550 nm, as this wavelength is cost-effective for laser sources.

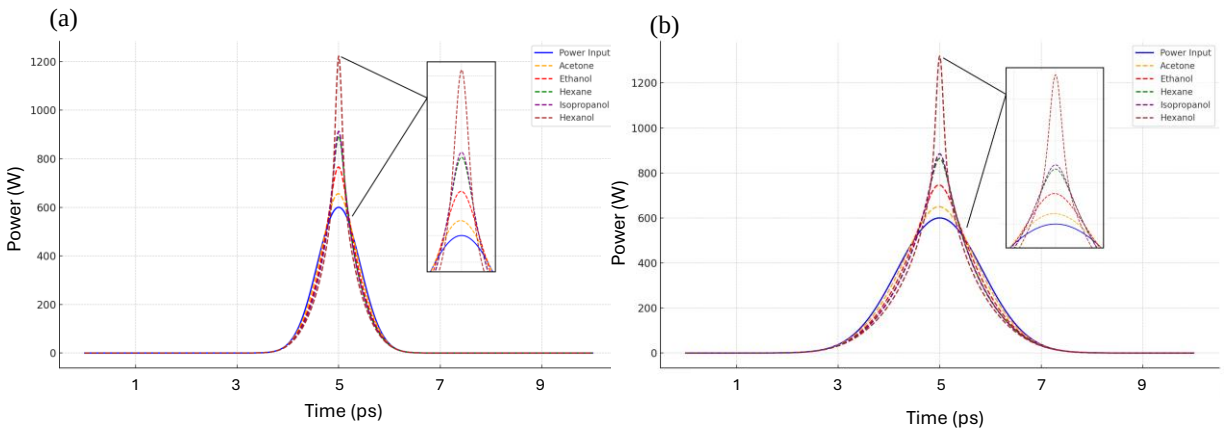

Figure 5.19: Comparison of the input pulse and the shape of pulse at the output for for sample pure solvents, when peak power of the input pulse is 600 W and FWHM is – a) 1ps , b)2ps.

Table 5.10: Power upsurge and compression sensitivity at the receiving end of HC-PCF for input pulse of 600 W and FWHM of 1ps and 2ps

Name of Pure solvent	**For input Pulse with peak power =600 W, FWHM= 1ps**		**For input Pulse with peak power =600 W, FWHM= 2ps**	
	Power Upsurge	Compression Sensitivity	Power Upsurge	Compression Sensitivity
Acetone	55.72	88%	49.96	89%
Ethanol	166.037	70%	146.526	73%
Hexane	293.985	54%	264.691	58%
Isopropanol	313.199	52%	284.873	56%
Hexanol	622.804	29%	719.33	24.50%

From *Figure 5.19* and *Table 5.10*, it is found that all the materials showed distinguished values of power upsurge and compression sensitivity at the output, making it easier for sensing. For input peak power 600 W and FWHM of 1 ps, the maximum power upsurge has been seen for Hexanol of 622.804 W and also the minimum compression sensitivity of 29%. For input pulse of 600W and FWHM of 2 ps, hexanol showed the extreme values. The minimum compression sensitivity being 24.5% and the maximum power upsurge being 719.33W.

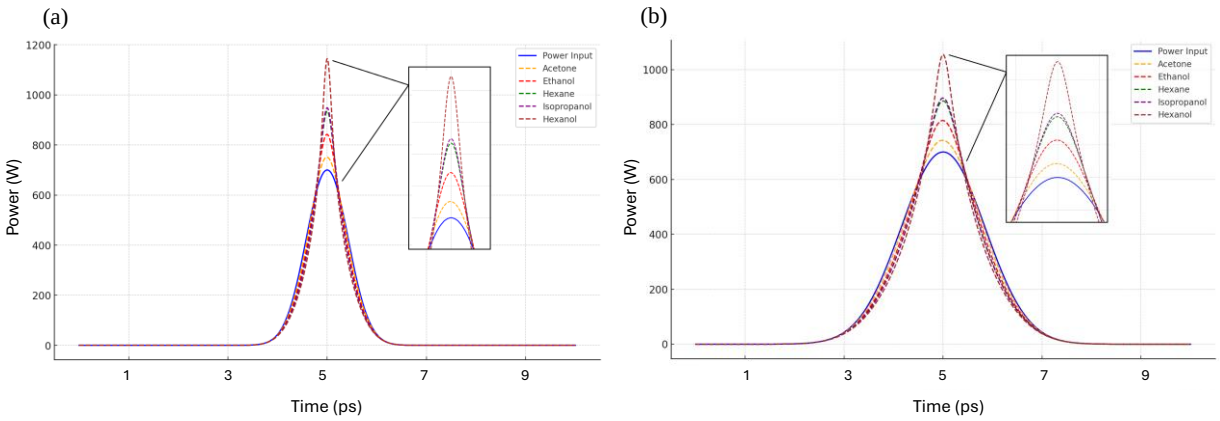

Figure 5.20: Comparison of the input pulse and the shape of pulse at the output for for sample pure solvents, when peak power of the input pulse is 700 W and FWHM is – a) 1ps , b)2ps.

Table 5.11: Power upsurge and compression sensitivity at the receiving end of HC-PCF for input pulse of 600 W and FWHM of 1ps and 2ps

Name of Pure solvent	**For input Pulse with peak power =700 W, FWHM= 1ps**		**For input Pulse with peak power =700 W, FWHM= 2ps**	
	Power Upsurge	Compression Sensitivity	Power Upsurge	Compression Sensitivity
Acetone	51.083	90%	42.397	91%
Ethanol	142.021	76%	114.577	80%
Hexane	234.847	66%	186.06	71%
Isopropanol	248.533	64%	196.665	70%
Hexanol	444.803	46%	354.946	54%

From *Figure 5.20* and *Table 5.11*, similar results have been obtained. All the solvents showed unique outputs, the extreme outputs have been received for hexanol. For input peak power 700 W and FWHM of 1 ps, the maximum power upsurge has been seen for Hexanol of 444.803 W and also the minimum compression sensitivity of 46%. For input pulse of 700W and FWHM of 2 ps, hexanol showed the extreme values. The minimum compression sensitivity being 54% and the maximum power upsurge being 354.94W.

In all four cases, an increase in power and unique compression sensitivity has been observed, confirming the reliability of the proposed HC-PCF design[43].

5.3.2 Sensing adulteration level is diesel through pulse compression using HC-PCF

Diesel, recognized for its efficiency, durability, and reduced emissions among fossil fuels, is extensively utilized in various applications. However, detecting adulteration in diesel presents a significant challenge, as it requires identifying contaminants without compromising safety or quality standards. The level of adulteration in diesel alters its refractive index, making it possible to apply our novel sensing technique by placing the samples in the core of an HC-PCF. This approach detects adulteration by monitoring changes in the shape of ultra-short pulses as they travel through the HC-PCF. The method leverages the fiber's nonlinear properties to observe alterations in pulse shape as they propagate through diesel-filled HC-PCF. By employing this technique, unique compression sensitivity and power enhancement have been achieved for diesel samples with varying adulteration levels, tailored to specific input configurations.

The diesel is generally adulterated using kerosene, here is a list given in the table below how the refractive index changes with the level of kerosene mixed.

Table 5.12: Refractive indices of diesel mixture with different levels of kerosene concentration

Kerosene Concentration in Diesel (%)	Refractive Index
0	1.455
20	1.4516
40	1.4482
60	1.4448
80	1.4414
100	1.4380

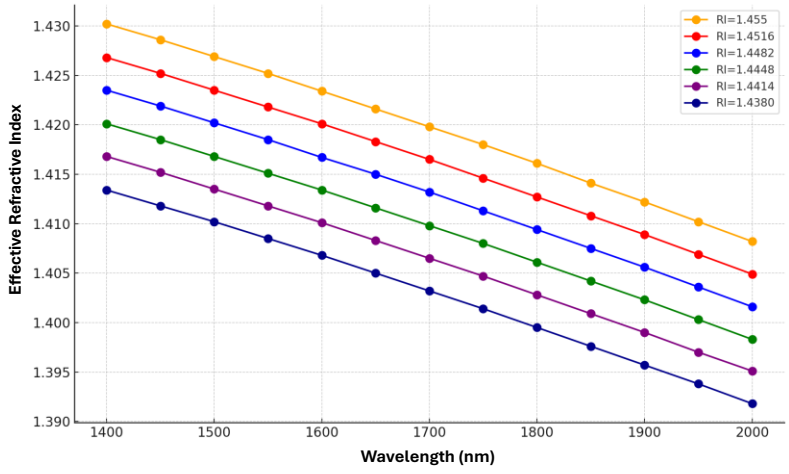

Figure 5.21: Effective refractive indices of HC-PCF filled with diesel samples with different kerosene concentrations.

The design of the HC-PCF was kept as it has been for the previous cases. The base material was also chosen silica like the previous cases. Initially using COMSOL Multiphysics, simulations were performed to extract information like- the Effective Refractive Index, Effective Area, and Power Fraction for each of the cases of HC-PCF filled with diesel of different adulteration level.

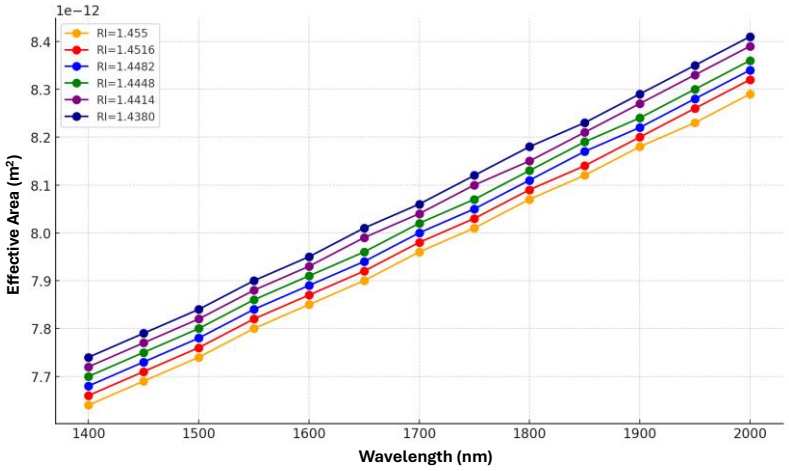

Figure 5.22: Effective area of HC-PCF filled with diesel samples with different kerosene concentrations.

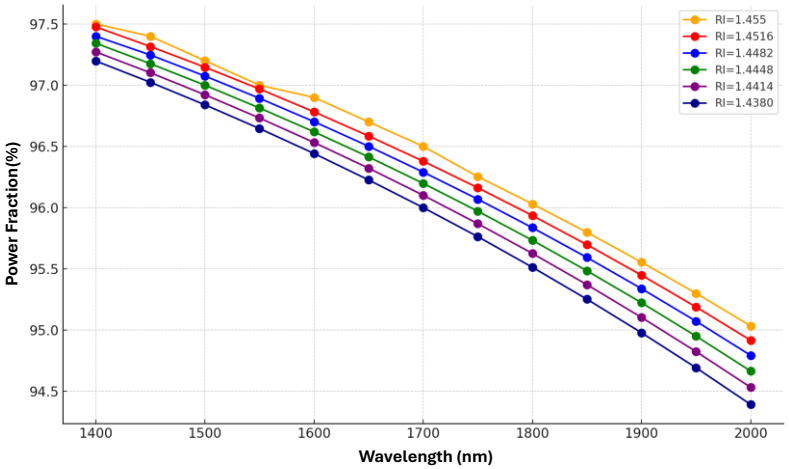

Figure 5.23: Power Fraction of HC-PCF filled with diesel samples with different kerosene concentrations.

From these extracted data, the other necessary parameters for solving NLSE using SSFM in MATLAB were calculated. They are shown in *Table 5.13*.

Table 5.13: Important parameter values extracted for analyzing change in the shape of ultra short pulse sent through HC-PCF

Concentration of Kerosene in Diesel	**Refractive Index**	**β_2 at 1550 nm** (s^2/m)	**β_3 at 1550 nm** (s^3/m)	**A_{eff} at 1550 nm** (m^2)	**γ** ($W^{-1}m^{-1}$)
0%	1.455	-6.08×10^{-26}	3.71×10^{-40}	7.80×10^{-12}	0.015591
20%	1.4516	-1.34×10^{-25}	-3.71×10^{-41}	7.82×10^{-12}	0.015671
40%	1.4482	-9.87×10^{-26}	1.83×10^{-40}	7.84×10^{-12}	0.015512
60%	1.4448	-8.92×10^{-26}	1.99×10^{-40}	7.86×10^{-12}	0.015472
80%	1.4414	-7.78×10^{-25}	4.63×10^{-40}	7.88×10^{-12}	0.015433
100%	1.4380	-1.32×10^{-25}	-2.05×10^{-40}	7.90×10^{-12}	0.015394

For this case keeping the constraints of fission length ($L_{fission} > L$) and soliton number ($N > 1$) , the fiber length was adjusted. Additionally, both pulse width and input power were varied. The pulse width was adjusted to 1 ps, 2 ps, and 3 ps, while input power levels of 400W and 500W were used to observe the overall behavior.

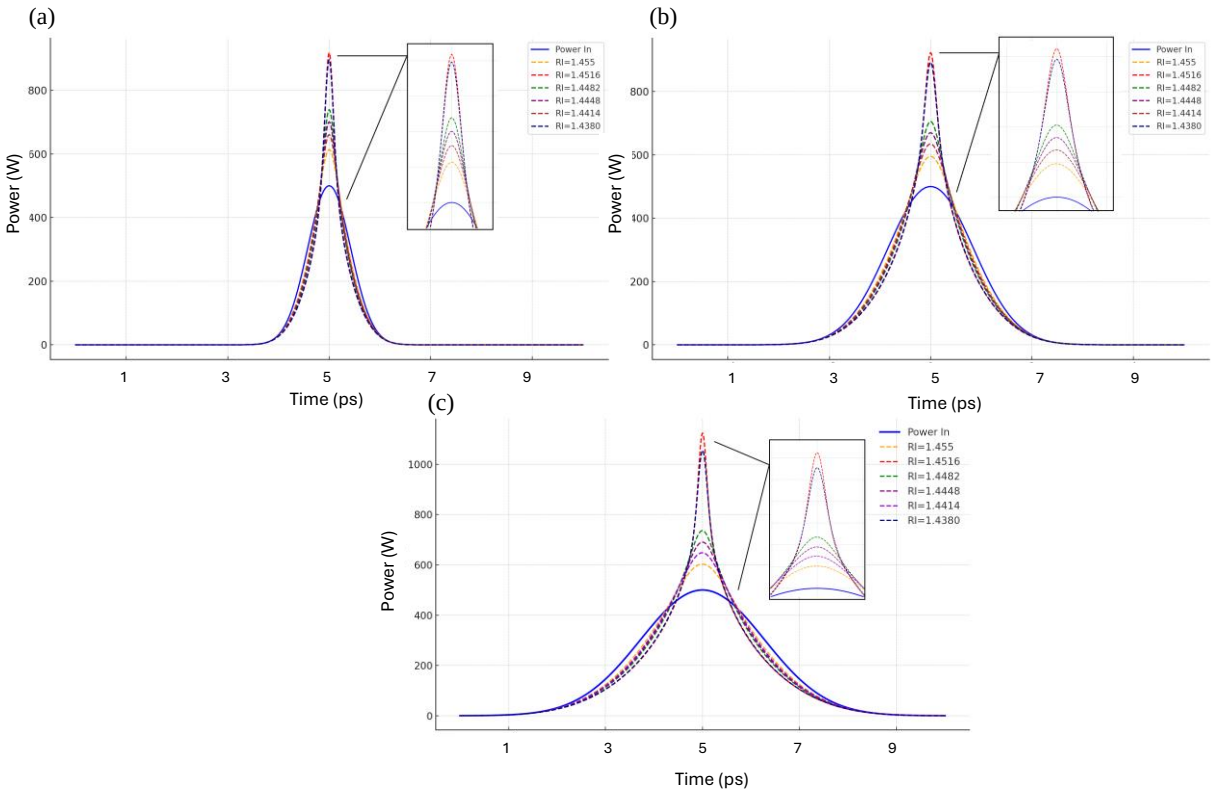

Figure 5.24: Shape of the pulse at the receiving end as it passed through HC-PCF filled with diesel sample with varying adulteration level for input power 500W and pulse width a) 1ps, b) 2ps, c) 3ps.

Table 5.14: Compression Sensitivity and Power Upsurge at the receiving end of HC-PCF for the input pulse having 500W power and pulse width of 1ps, 2ps and 3ps.

Concentration of Kerosene in Diesel	For Input Power = 500W and Pulse width = 1ps		For Input Power = 500W and Pulse width = 2ps		For Input Power = 500 W and Pulse width = 3ps	
	Power Upsurge (W)	Compression Sensitivity (%)	Power Upsurge (W)	Compression Sensitivity (%)	Power Upsurge (W)	Compression Sensitivity (%)
0%	113.621	74	95.001	78	102.649	76.67
20%	481.4059457	36	422.867	36	623.862	23.34
40%	239.3654574	54	205.518	60	235.878	56
60%	200.938276	60	169.842	65	190.352	62.67
80%	160.7140224	66	134.632	71	148.031	68.67
100%	396.4026045	38	392.841	38	555.095	54.67

The HC-PCF filled with fuel samples were exposed to input power of 500W and pulse width was varied from 1ps to 3ps. The results can be seen from Figure 5.22, it shows that for this input configuration, the detection of fuel adulteration can be made quite conveniently. For each of these input configurations, Fiber length was chosen to be 0.35m, 0.65m and 1m. The sensitivity and power upsurge for each of the samples for each input configuration are presented in Table 5.14.

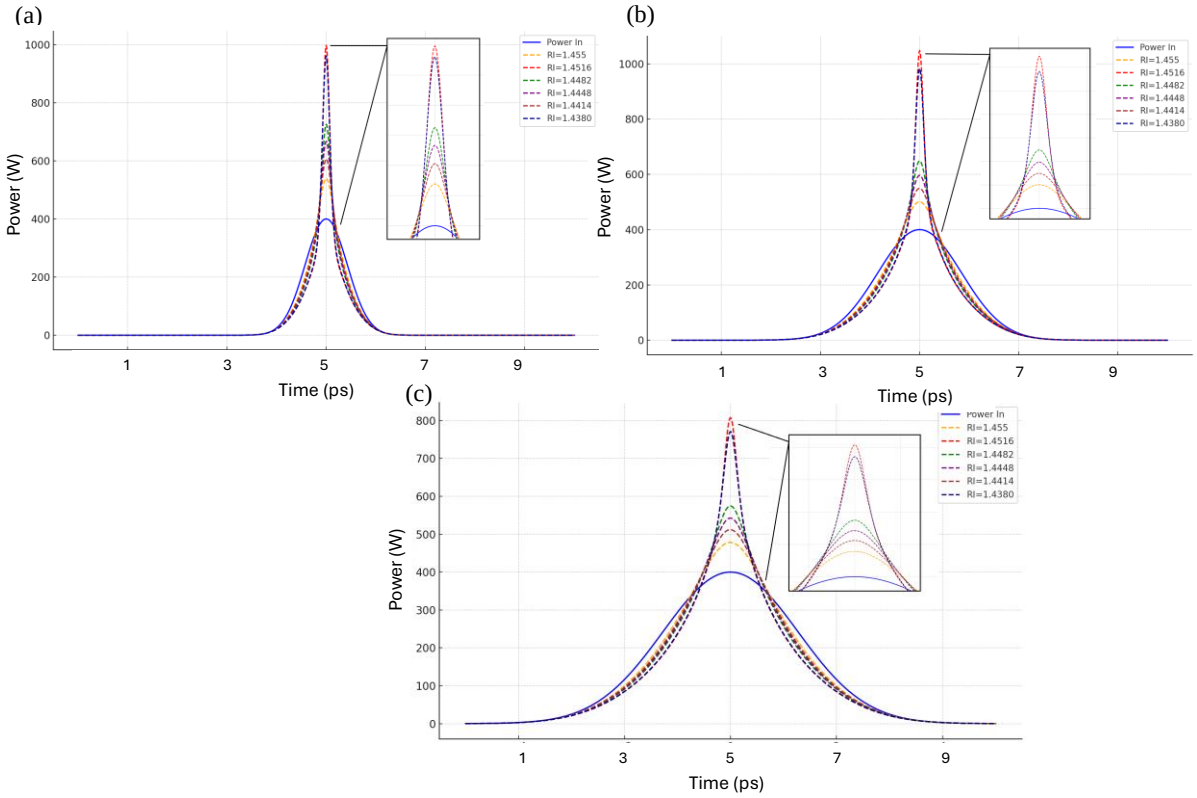

Figure 5.25: Shape of the pulse at the receiving end as it passed through HC-PCF filled with diesel sample with varying adulteration level for input power 400W and pulse width a) 1ps, b) 2ps, c) 3ps.

Table 5.15: Compression Sensitivity and Power Upsurge at the receiving end of HC-PCF for the input pulse having 400W power and pulse width of 1ps, 2ps and 3ps.

Concentration of Kerosene in Diesel	**For Input Power = 400W and Pulse width = 1ps**		**For Input Power = 400W and Pulse width = 2ps**		**For Input Power = 400 W and Pulse width = 3ps**	
	Power Upsurge (W)	Compression Sensitivity (%)	Power Upsurge (W)	Compression Sensitivity (%)	Power Upsurge (W)	Compression Sensitivity (%)
0%	138.832	64.4	100.585	73	78.302	78
20%	596.719	22	648.072	16	407.576	30.367
40%	325.62	37	248.64	47	174.58	58.67
60%	266.64	44	196.468	55	142.515	64.34
80%	206.204	50	149.16	63	111.946	70.34
100%	560.665	24	583.086	18	370.908	33.67

Again, the HC-PCF filled with fuel samples were exposed to input power of 400W and pulse width was varied from 1ps to 3ps. The results can be seen from *Figure 5.25*, it demonstrates that for this input configuration, the detection of fuel adulteration can also be made quite efficiently. For each of these input configurations, Fiber length was chosen to be 0.45m, 0.8m and 1.1m. The sensitivity and power upsurge for each of the samples for each input configuration are presented in *Table 5.15*.

From the results obtained, it is quite evident that fuel adulteration can indeed be detected from observing the shape of ultra short pulse as it propagates through the HC-PCF. The power upsurge and pulse compression are unique for each fuel sample. Both of these output parameters can be observed from the tables and the figures presented. If an experimental setup (*Figure 4.9*) would be prepared, then an autocorrelator and power meter would be required to measure these two quantities[44]. Unlike the recent works based on HC-PCF, this proposed sensing mechanism will not require a variety of output parameters; like- Relative sensitivity, EML, Birefringence, Numerical Aperture etc. to sense sample materials, which makes the proposed method less complex compared to them[51],[55]-[58],[60].

Chapter 6
Concluding Remarks

In this thesis, the development and implementation of a novel sensing technique utilizing HC-PCFs to detect and analyze materials with varying refractive indices have been explored. The limitations of existing sensing techniques are addressed by simplifying the decision-making process and improving the practicality and efficiency of HC-PCF-based sensing systems.

6.1 Summary of the Thesis

Here is a summary of the thesis-

Overview of Photonic Crystal Fibers

The thesis began by providing an in-depth overview of photonic crystal fibers, specifically HC-PCFs, which leverage their unique structure for guiding light through a hollow core. The properties of HC-PCFs allow for a significant reduction in light interaction with the solid fiber material, making them ideal for applications that require precise material sensing, particularly in environments where conventional sensors might be ineffective due to interference or material constraints.

Nonlinear Optical Effects and Ultra-Short Pulse Propagation

A central theme of this work has been the investigation of nonlinear optical effects, such as self-phase modulation, four-wave mixing, and soliton generation. These phenomena arise when ultra-short light pulses, typically in the femtosecond regime, propagate through the HC-PCF. The interaction between the light and the material filling the core results in characteristic changes in pulse behavior, which serve as the foundation for the sensing technique proposed in this thesis.

Existing Techniques vs. Simplified Approach

Current HC-PCF-based sensing methods often require the analysis of multiple parameters—such as numerical aperture, relative sensitivity, confinement loss, and effective area—to arrive at a decision. This approach, while effective, can be cumbersome, especially in real-world applications where simplicity, speed, and accuracy are paramount.

In contrast, the novel technique proposed in this thesis focuses on just two critical parameters: compression sensitivity and power upsurge. These two factors are sufficient to detect and distinguish materials with different refractive indices, making the method more straightforward to implement while still maintaining high sensitivity and accuracy. By analyzing how an ultra-short pulse is compressed and how the power

output increases as the pulse travels through the HC-PCF, we can reliably identify the material filling the core.

Practical Applications and Future Outlook

The simplicity of this approach makes it suitable for a wide range of applications, including environmental monitoring, chemical detection, and biomedical diagnostics. The potential to apply this sensing technique in real-world scenarios, such as detecting impurities in fuel or identifying chemical compositions in industrial processes, offers significant advantages over traditional methods.

Moving forward, this research opens the door for further optimization of HC-PCF designs to enhance sensitivity and efficiency even more. Future work could also explore the integration of this sensing mechanism into portable, real-time devices that could be deployed across various industries.

6.2 Conclusion

In conclusion, this thesis has contributed to the field of photonic crystal fiber technology by proposing and validating a novel, simplified sensing method based on compression sensitivity and power upsurge. The complexity of HC-PCF-based sensors has been reduced, making them more accessible and practical for various applications. The potential of this sensing method for reliable and efficient material detection has been demonstrated through theoretical analysis, numerical simulations, and proposed experimental setups, paving the way for its application in industrial and scientific domains.

References

[1] K. Amsalu and S. Palani, "A review on photonics and its applications," *Mater Today Proc*, vol. 33, pp. 3372–3377, 2020, doi: https://doi.org/10.1016/j.matpr.2020.05.184.

[2] M. Girtan, "Is photonics the new electronics?," *Materials Today*, vol. 17, pp. 100–101, Sep. 2014, doi: 10.1016/j.mattod.2014.03.003.

[3] M. S. Moreolo, L. Nadal, J. M. Fabrega, and J. Vílchez, "Photonic and Quantum Communication Technologies for Optical Networks Evolution," in *2023 23rd International Conference on Transparent Optical Networks (ICTON)*, 2023, pp. 1–4. doi: 10.1109/ICTON59386.2023.10207227.

[4] M. S. Moreolo *et al.*, "Programmable VCSEL-based photonic system architecture for future agile Tb/s metro networks," *Journal of Optical Communications and Networking*, vol. 13, no. 2, pp. A187–A199, 2021, doi: 10.1364/JOCN.411964.

[5] Y. Shi *et al.*, "Silicon photonics for high-capacity data communications," *Photonics Res*, vol. 10, no. 9, pp. A106–A134, 2022, doi: 10.1364/PRJ.456772.

[6] J.-H. Kim, S. Aghaeimeibodi, J. Carolan, D. Englund, and E. Waks, "Hybrid integration methods for on-chip quantum photonics," *Optica*, vol. 7, no. 4, pp. 291–308, 2020, doi: 10.1364/OPTICA.384118.

[7] L. Feng *et al.*, "Silicon photonic devices for scalable quantum information applications," *Photonics Res*, vol. 10, no. 10, pp. A135–A153, 2022, doi: 10.1364/PRJ.464808.

[8] T. Heindel, J.-H. Kim, N. Gregersen, A. Rastelli, and S. Reitzenstein, "Quantum dots for photonic quantum information technology," *Adv Opt Photonics*, vol. 15, no. 3, pp. 613–738, 2023, doi: 10.1364/AOP.490091.

[9] P. S, A. Sivasangari, P. Ajitha, S. Lalithakumari, A. Sridevi, and S. K. Danasegaran, "Design and performance analysis of smart photonic sensors for industrial applications," *Current Applied Physics*, vol. 39, pp. 183–189, 2022, doi: https://doi.org/10.1016/j.cap.2022.04.006.

[10] N. L. Kazanskiy, S. N. Khonina, and M. A. Butt, "Plasmonic sensors based on Metal-insulator-metal waveguides for refractive index sensing applications: A brief review," *Physica E Low Dimens Syst Nanostruct*, vol. 117, p. 113798, 2020, doi: https://doi.org/10.1016/j.physe.2019.113798.

[11] A. Mendez, "Photonic Sensing Technology in the Energy Sector," in *Latin America Optics and Photonics Conference*, in OSA Technical Digest (online). Sao Sebastiao: Optica Publishing Group, 2012, p. LS3B.1. doi: 10.1364/LAOP.2012.LS3B.1.

[12] S. Khani and M. Hayati, "Optical biosensors using plasmonic and photonic crystal band-gap structures for the detection of basal cell cancer," *Sci Rep*, vol. 12, no. 1, Dec. 2022, doi: 10.1038/s41598-022-09213-w.

[13] Vikas and P. Saccomandi, "Antimonene-Coated Uniform-Waist Tapered Fiber Optic Surface Plasmon Resonance Biosensor for the Detection of Cancerous Cells: Design and Optimization," *ACS Omega*, vol. 8, no. 5, pp. 4627–4638, Feb. 2023, doi: 10.1021/acsomega.2c06037.

[14] J. E. Anderson and J. E. Jackson, "Theory and application of pulsed laser welding," *Weld J*, vol. 44, pp. 1018–1026, Jan. 1965.

[15] T. Maiman, "Stimulated optical radiation in ruby masers," *Nature*, vol. 187, pp. 493–494, Aug. 1960, doi: 10.1038/187493a0.

[16] G. Klauminzer, “Twenty years of commercial lasers—a capsule history,” *Laser Focus/Electro-optics*, vol. 20, pp. 54–79, Dec. 1984.

[17] N. Taylor and N. Bloembergen, “Laser: The Inventor, the Nobel Laureate, and the Thirty-Year Patent War,” *Physics Today - PHYS TODAY*, vol. 12, Sep. 2001, doi: 10.1063/1.1420516.

[18] A. Bernatskyi and V. Khaskin, “The history of the creation of lasers and analysis of the impact of their application in the material processing on the development of certain industries,” *History of science and technology*, vol. 11, pp. 125–149, Jun. 2021, doi: 10.32703/2415-7422-2021-11-1-125-149.

[19] K. C. Kao, G. A. Hockham, and I. E. E. Synopsis, “Dielectric-fibre surface waveguides for optical frequencies "I Jo(M i) for H Om modes u 2 K 0 (w 2),” 1966.

[20] H. H. HOPKINS and N. S. KAPANY, “A Flexible Fibrescope, using Static Scanning,” *Nature*, vol. 173, no. 4392, pp. 39–41, 1954, doi: 10.1038/173039b0.

[21] K. P. Singh, “In memory of Narinder Singh Kapany,” *Nat Photonics*, vol. 15, no. 6, pp. 403–404, 2021, doi: 10.1038/s41566-021-00812-z.

[22] N. S. KAPANY, “High-Resolution Fibre Optics Using Sub-Micron Multiple Fibres,” *Nature*, vol. 184, no. 4690, pp. 881–883, 1959, doi: 10.1038/184881a0.

[23] A. E. Willner, S. Khaleghi, M. R. Chitgarha, and O. F. Yilmaz, “All-Optical Signal Processing,” *Journal of Lightwave Technology*, vol. 32, no. 4, pp. 660–680, 2014, doi: 10.1109/JLT.2013.2287219.

[24] A. Zanella, N. Bui, A. Castellani, L. Vangelista, and M. Zorzi, “Internet of Things for Smart Cities,” *IEEE Internet Things J*, vol. 1, no. 1, pp. 22–32, 2014, doi: 10.1109/JIOT.2014.2306328.

[25] S. Addanki, I. S. Amiri, and P. Yupapin, “Review of optical fibers-introduction and applications in fiber lasers,” *Results Phys*, vol. 10, pp. 743–750, 2018, doi: https://doi.org/10.1016/j.rinp.2018.07.028.

[26] J. Wang, Y. Han, Z. Cao, X. Xu, J. Zhang, and F. Xiao, “Applications of optical fiber sensor in pavement Engineering: A review,” *Constr Build Mater*, vol. 400, p. 132713, 2023, doi: https://doi.org/10.1016/j.conbuildmat.2023.132713.

[27] Y. Liu, J. Xie, S. Liu, Y. Zhao, Y. Zhu, and G. Qi, “Research on the methodology of development and calibration of flexible encapsulated fiber Bragg grating sensors,” *Measurement*, vol. 201, p. 111730, 2022, doi: https://doi.org/10.1016/j.measurement.2022.111730.

[28] A. D. Kersey, D. A. Jackson, and M. Corke, “A simple fibre Fabry-Perot sensor,” *Opt Commun*, vol. 45, no. 2, pp. 71–74, 1983, doi: https://doi.org/10.1016/0030-4018(83)90047-0.

[29] M. de Vries, V. Arya, S. Meller, S. F. Masri, and R. O. Claus, “Implementation of EFPI-based optical-fiber sensor instrumentation for the NDE of concrete structures,” *Cem Concr Compos*, vol. 19, no. 1, pp. 69–79, 1997, doi: https://doi.org/10.1016/S0958-9465(96)00043-1.

[30] L. Jiao, N. Zhong, X. Zhao, S. Ma, X. Fu, and D. Dong, “Recent advances in fiber-optic evanescent wave sensors for monitoring organic and inorganic pollutants in water,” *TrAC Trends in Analytical Chemistry*, vol. 127, p. 115892, 2020, doi: https://doi.org/10.1016/j.trac.2020.115892.

[31] G. Stewart, W. Jin, and B. Culshaw, “Prospects for fibre-optic evanescent-field gas sensors using absorption in the near-infrared,” *Sens Actuators B Chem*, vol. 38, no. 1, pp. 42–47, 1997, doi: https://doi.org/10.1016/S0925-4005(97)80169-4.

[32] Alan Rogers, “Distributed optical-fibre sensing,” *Meas Sci Technol*, vol. 10, no. 8, p. R75, 1999, doi: 10.1088/0957-0233/10/8/201.

[33] P. Lu *et al.*, “Distributed optical fiber sensing: Review and perspective,” Dec. 01, 2019, *American Institute of Physics Inc.* doi: 10.1063/1.5113955.

[34] E. F. de Macedo, L. S. Nascimento, Y. Hou, R. Mathey, and D. B. Tada, “Simultaneous detection of CA-125 and mesothelin by gold nanoparticles in surface plasmon resonance,” *Sens Biosensing Res*, vol. 43, p. 100609, 2024, doi: https://doi.org/10.1016/j.sbsr.2023.100609.

[35] C. M. Miyazaki, F. M. Shimizu, and M. Ferreira, “6 - Surface Plasmon Resonance (SPR) for Sensors and Biosensors,” in *Nanocharacterization Techniques*, A. L. Da Róz, M. Ferreira, F. de Lima Leite, and O. N. Oliveira, Eds., William Andrew Publishing, 2017, pp. 183–200. doi: https://doi.org/10.1016/B978-0-323-49778-7.00006-0.

[36] A. S. Kushwaha, A. Kumar, R. Kumar, and S. K. Srivastava, “A study of surface plasmon resonance (SPR) based biosensor with improved sensitivity,” *Photonics Nanostruct*, vol. 31, pp. 99–106, 2018, doi: https://doi.org/10.1016/j.photonics.2018.06.003.

[37] Y. Yu *et al.*, “Some features of the photonic crystal fiber temperature sensor with liquid ethanol filling,” *Opt Express*, vol. 18, no. 15, pp. 15383–15388, 2010, doi: 10.1364/OE.18.015383.

[38] M. J. Bin Murshed Leon and A. S. Disha, “A simple structure of PCF based sensor for sensing sulfur dioxide gas with high sensitivity and better birefringence,” *Sensors International*, vol. 2, p. 100115, 2021, doi: https://doi.org/10.1016/j.sintl.2021.100115.

[39] H. Ademgil and S. Haxha, “PCF Based Sensor with High Sensitivity, High Birefringence and Low Confinement Losses for Liquid Analyte Sensing Applications,” *Sensors*, vol. 15, no. 12, pp. 31833–31842, 2015, doi: 10.3390/s151229891.

[40] P. St. J. Russell, P. Hölzer, W. Chang, A. Abdolvand, and J. C. Travers, “Hollow-core photonic crystal fibres for gas-based nonlinear optics,” *Nat Photonics*, vol. 8, no. 4, pp. 278–286, 2014, doi: 10.1038/nphoton.2013.312.

[41] J. C. Travers, W. Chang, J. Nold, N. Y. Joly, and P. St. J. Russell, “Ultrafast nonlinear optics in gas-filled hollow-core photonic crystal fibers [Invited],” *Journal of the Optical Society of America B*, vol. 28, no. 12, pp. A11–A26, 2011, doi: 10.1364/JOSAB.28.000A11.

[42] S. M. Mahbub, M. H. M. Shamim, and R. H. Sagor, “Gas Detection Utilizing Soliton Effect Pulse Compression in a Hollow Core Photonic Crystal Fiber,” in *2024 6th International Conference on Electrical Engineering and Information & Communication Technology (ICEEICT)*, 2024, pp. 308–312. doi: 10.1109/ICEEICT62016.2024.10534440.

[43] S. M. Mahbub, A. A. M. Nafiz, A. A. Protiva, M. Tamim, and R. Rahad, “Ultra-short pulse: A comprehensive way of sensing pure solvents through hollow core photonic crystal fiber sensor,” *Opt Mater (Amst)*, vol. 156, p. 116028, 2024, doi: https://doi.org/10.1016/j.optmat.2024.116028.

[44] M. Mahbub, A. Al, M. Nafiz, A. Protiva, M. Tamim, and R. Hasan Sagor, “Sensing fuel adulteration level in diesel analyzing the change in shape of ultra-short pulse sent through Hollow Core Photonic Crystal Fiber,” 2024. [Online]. Available: https://ssrn.com/abstract=4765839

[45] A. L. Gaeta, “Nonlinear optics in hollow-core photonic crystal fibers,” in *CLEO/Europe. 2005 Conference on Lasers and Electro-Optics Europe, 2005.*, 2005, pp. 199–200. doi: 10.1109/CLEOE.2005.1567986.

[46] P. Biswas and S. Ghosh, “A Specialty Endless-Core Photonic Bandgap Fiber with Ultra-wide Bandwidth for Short Pulse Propagation,” in *Frontiers in Optics / Laser Science*, B. Lee Mazzali C. Corwin K. and Jason Jones R., Ed., in OSA Technical Digest. Washington, DC: Optica Publishing Group, 2020, p. JTu1A.29. doi: 10.1364/FIO.2020.JTu1A.29.

[47] D. Bermudez, “Propagation of Ultra-Short Higher-Order Solitons in a Photonic Crystal Fiber,” in *Journal of Physics: Conference Series*, Institute of Physics Publishing, Apr. 2016. doi: 10.1088/1742-6596/698/1/012017.

[48] J. Lægsgaard, “Soliton formation in hollow-core photonic bandgap fibers,” *Applied Physics B*, vol. 95, no. 2, pp. 293–300, 2009, doi: 10.1007/s00340-008-3357-z.

[49] X. Hu *et al.*, “Nonlinear chirped-pulse propagation and supercontinuum generation in photonic crystal fibers,” *Appl Opt*, vol. 49, no. 26, pp. 4984–4989, 2010, doi: 10.1364/AO.49.004984.

[50] X. Qi *et al.*, “Understanding Nonlinear Pulse Propagation in Liquid Strand-Based Photonic Bandgap Fibers,” *Crystals (Basel)*, vol. 11, no. 3, 2021, doi: 10.3390/cryst11030305.

[51] R. Yu, Y. Chen, L. Shui, and L. Xiao, “Hollow-core photonic crystal fiber gas sensing,” May 02, 2020, *MDPI AG*. doi: 10.3390/s20102996.

[52] S. Eilzer and B. Wedel, “Hollow Core Optical Fibers for Industrial Ultra Short Pulse Laser Beam Delivery Applications,” *Fibers*, vol. 6, no. 4, 2018, doi: 10.3390/fib6040080.

[53] M. Harvey, R. Cisek, and D. Tokarz, “Spectral Broadening of Ultrashort Pulses by Nonlinear Optical Effects in Photonic Crystal Fiber,” in *2021 Photonics North (PN)*, 2021, pp. 1–2. doi: 10.1109/PN52152.2021.9597897.

[54] C. Markos, J. C. Travers, A. Abdolvand, B. J. Eggleton, and O. Bang, “Hybrid photonic-crystal fiber,” Mar. 2019, doi: 10.1103/RevModPhys.89.045003.

[55] S. Ahmed, J. R. Mou, M. A. Mollah, and N. Debnath, “Hollow-core Photonic Crystal Fiber Sensor for Refractive Index Sensing,” in *2019 IEEE International Conference on Telecommunications and Photonics (ICTP)*, 2019, pp. 1–4. doi: 10.1109/ICTP48844.2019.9041790.

[56] N. F. Baharin *et al.*, “HOLLOW-CORE PHOTONIC CRYSTAL FIBER REFRACTIVE INDEX SENSOR BASED ON MODAL INTERFERENCE,” vol. 11, no. 9, 2016, [Online]. Available: www.arpnjournals.com

[57] R. Senthil, U. Anand, and P. Krishnan, “Hollow-core high-sensitive photonic crystal fiber for liquid-/gas-sensing applications,” *Applied Physics A*, vol. 127, no. 4, p. 282, 2021, doi: 10.1007/s00339-021-04417-9.

[58] Md. A. Habib, Md. S. Anower, L. F. Abdulrazak, and Md. S. Reza, “Hollow core photonic crystal fiber for chemical identification in terahertz regime,” *Optical Fiber Technology*, vol. 52, p. 101933, 2019, doi: https://doi.org/10.1016/j.yofte.2019.101933.

[59] M. M. A. Eid, M. A. Habib, M. S. Anower, and A. N. Z. Rashed, “Hollow Core Photonic Crystal Fiber (PCF)–Based Optical Sensor for Blood Component Detection in Terahertz Spectrum,” *Brazilian Journal of Physics*, vol. 51, no. 4, pp. 1017–1025, Aug. 2021, doi: 10.1007/s13538-021-00906-7.

[60] Md. R. Sardar, M. Faisal, and K. Ahmed, “Simple hollow core photonic crystal fiber for monitoring carbon dioxide gas with very high accuracy,” *Sens Biosensing Res*, vol. 31, p. 100401, 2021, doi: https://doi.org/10.1016/j.sbsr.2021.100401.

[61] M. Khelladi, “Study and Synthesis of the Propagation of Ultrashort Laser Pulses in Medias: Fused Silica, Photonic Crystal Fiber, Air Silica and Hollow Core,” 2022, doi: 10.21203/rs.3.rs-2165945/v1.

[62] P. J. Mosley, W. C. Huang, M. G. Welch, B. J. Mangan, W. J. Wadsworth, and J. C. Knight, “Ultrashort pulse compression and delivery in a hollow-core photonic crystal fiber at 540 nm wavelength,” *Opt Lett*, vol. 35, no. 21, pp. 3589–3591, 2010, doi: 10.1364/OL.35.003589.

[63] G. P. Agrawal, “Chapter 2 - Pulse propagation in fibers,” in *Nonlinear Fiber Optics (Sixth Edition)*, Sixth Edition., G. P. Agrawal, Ed., Academic Press, 2019, pp. 27–55. doi: https://doi.org/10.1016/B978-0-12-817042-7.00009-9.

[64] G. P. Agrawal, “Chapter 3 - Group-velocity dispersion,” in *Nonlinear Fiber Optics (Sixth Edition)*, Sixth Edition., G. P. Agrawal, Ed., Academic Press, 2019, pp. 57–84. doi: https://doi.org/10.1016/B978-0-12-817042-7.00010-5.

[65] S. Garzo and M. Mendoza, “Simulation for fiber optics pulse propagation through a numerical solution of the Nonlinear Schrödinger Equation.”

[66] R. W. Boyd, “Chapter 13 - Ultrafast and Intense-Field Nonlinear Optics,” in *Nonlinear Optics (Third Edition)*, R. W. Boyd, Ed., Burlington: Academic Press, 2008, pp. 561–587. doi: https://doi.org/10.1016/B978-0-12-369470-6.00013-7.

[67] “Thorlabs PCF Specification.” Accessed: Dec. 31, 2023. [Online]. Available: https://www.thorlabs.com/newgrouppage9.cfm?objectgroup_id=912

[68] Mark G Allen, “Diode laser absorption sensors for gas-dynamic and combustion flows,” *Meas Sci Technol*, vol. 9, no. 4, p. 545, 1998, doi: 10.1088/0957-0233/9/4/001.

[69] U. Yaqoob and M. I. Younis, “Chemical Gas Sensors: Recent Developments, Challenges, and the Potential of Machine Learning—A Review,” *Sensors*, vol. 21, no. 8, 2021, doi: 10.3390/s21082877.

[70] T. Akamatsu, T. Itoh, and W. Shin, “Mixed-Potential Gas Sensors Using an Electrolyte Consisting of Zinc Phosphate Glass and Benzimidazole,” *Sensors*, vol. 17, no. 1, 2017, doi: 10.3390/s17010097.

[71] M. Elsherif *et al.*, “Optical Fiber Sensors: Working Principle, Applications, and Limitations,” *Adv Photonics Res*, vol. 3, no. 11, Nov. 2022, doi: 10.1002/adpr.202100371.

[72] M.-J. Li, “Optical Fiber Evolution Over the Past 5 Decades,” in *Frontiers in Optics / Laser Science*, Optica Publishing Group, 2020, p. FM4D.1. doi: 10.1364/FIO.2020.FM4D.1.

[73] S. K. Dubey, A. Kumar, A. Kumar, A. Pathak, and S. K. Srivastava, “A study of highly sensitive D-shaped optical fiber surface plasmon resonance based refractive index sensor using grating structures of Ag-TiO2 and Ag-SnO2,” *Optik (Stuttg)*, vol. 252, p. 168527, 2022, doi: https://doi.org/10.1016/j.ijleo.2021.168527.

[74] H. Liang, T. Shen, Y. Feng, H. Liu, and W. Han, “A D-Shaped Photonic Crystal Fiber Refractive Index Sensor Coated with Graphene and Zinc Oxide,” *Sensors*, vol. 21, no. 1, 2021, doi: 10.3390/s21010071.

[75] R. Paschotta, Article on Sellmeier formula in the *Encyclopedia of Laser Physics and Technology*, 1. edition October 2008, Wiley-VCH, ISBN 978-3-527-40828-3

[76] A. Bideau-Mehu, Y. Guern, R. Abjean, and A. Johannin-Gilles, “Interferometric determination of the refractive index of carbon dioxide in the ultraviolet region,” *Opt Commun*, vol. 9, no. 4, pp. 432–434, 1973, doi: https://doi.org/10.1016/0030-4018(73)90289-7.

[77] R. Rollefson and R. Havens, “Index of Refraction of Methane in the Infra-Red and the Dipole Moment of the CH Bond,” *Physical Review*, vol. 57, no. 8, pp. 710–717, Apr. 1940, doi: 10.1103/PhysRev.57.710.

[78] A. Bideau-Mehu, Y. Guern, R. Abjean, and A. Johannin-Gilles, “Measurement of refractive indices of neon, argon, krypton and xenon in the 253.7–140.4 nm wavelength range. Dispersion relations and estimated oscillator strengths of the resonance lines,” *J Quant Spectrosc Radiat Transf*, vol. 25, no. 5, pp. 395–402, 1981, doi: https://doi.org/10.1016/0022-4073(81)90057-1.

[79] A. Bostani, A. Tehranchi, and R. Kashyap, “Super-tunable, broadband upconversion of a high-power CW laser in an engineered nonlinear crystal,” *Sci Rep*, vol. 7, no. 1, Dec. 2017, doi: 10.1038/s41598-017-00974-3.

[80] S. A. Mousavi *et al.*, “Nonlinear dynamic of picosecond pulse propagation in atmospheric air-filled hollow core fibers,” *Opt Express*, vol. 26, no. 7, p. 8866, Apr. 2018, doi: 10.1364/oe.26.008866.

[81] Z. Liu *et al.*, “Reflective-distributed SPR sensor based on twin-core fiber,” *Opt Commun*, vol. 366, pp. 107–111, 2016, doi: https://doi.org/10.1016/j.optcom.2015.12.018.

[82] Wright, S.F.; Zadrazil, I.; Markides, C.N. (2017). "A review of solid–fluid selection options for optical-based measurements in single-phase liquid, two-phase liquid–liquid and multiphase solid–liquid flows". *Experiments in Fluids*. **58** (9): 108. Bibcode:2017ExFl...58..108W. doi:10.1007/s00348-017-2386-y. hdl:10044/1/49407.

[83] *184 Silicone Elastomer" (PDF) (Product Information). Dow Corning. Retrieved 11 December 2012.*

[84] "Manual for Sugar Solution Prism" (PDF). A/S S. Frederiksen. 3 August 2005. Archived from the original (PDF) on 3 March 2016. Retrieved 21 March 2012.

[85] J. Volk, T. Le Grand, I. Bársony, J. Gombkötő, and J. J. Ramsden, “Porous silicon multilayer stack for sensitive refractive index determination of pure solvents,” *J Phys D Appl Phys*, vol. 38, no. 8, p. 1313, 2005, doi: 10.1088/0022-3727/38/8/032.

[86] W. E. Luttrell and A. L. LaGrow, “Acetone,” 2014, *Elsevier Inc.* doi: 10.1016/j.jchas.2014.03.006.

[87] M. Alshareef *et al.*, “Optical Detection of Acetone Using ‘ Turn-Off’ Fluorescent Rice Straw Based Cellulose Carbon Dots Imprinted onto Paper Dipstick for Diabetes Monitoring,” *ACS Omega*, 2022, doi: 10.1021/acsomega.2c01492.

[88] C. Togbé, P. Dagaut, A. Mzé-Ahmed, P. Diévart, F. Halter, and F. Foucher, “Experimental and detailed kinetic modeling study of 1-hexanol oxidation in a pressurized jet-stirred reactor and a combustion bomb,” *Energy and Fuels*, vol. 24, no. 11, pp. 5859–5875, Nov. 2010, doi: 10.1021/ef101255w

[89] C. Cravotto *et al.*, “Towards Substitution of Hexane as Extraction Solvent of Food Products and Ingredients with No Regrets,” Nov. 01, 2022, *MDPI*. doi: 10.3390/foods11213412.

[90] N. M. Saad, E.-S. M. El-Rabaie, and A. A. M. Khalaf, “Photonic Crystal Fiber Sensors, Literature Review, Challenges, and Some Novel Trends.”

Appendix

A. List of Abbreviation of Technical Terms

PCF – Photonic Crystal Fiber

HC-PCF – Hollow Core Photonic Crystal Fiber

MUS- Material Under sensing

SPR- Surface plasmon resonance

PBG- Photonic Bandgap

Neff- Effective Refractive index

RI- Refractive Index

NLSE-Nonlinear Schrödinger equation

SSFM- Split Step Fourier Method

SPM- Self-phase modulation

XPM- cross-phase modulation

FWM- Four-wave mixing

FWHM- Full width half maximum

B. List of Publications based on the works of this dissertation

[1] S. M. Mahbub, M. H. M. Shamim, and R. H. Sagor, “Gas Detection Utilizing Soliton Effect Pulse Compression in a Hollow Core Photonic Crystal Fiber,” in *2024 6th International Conference on Electrical Engineering and Information & Communication Technology (ICEEICT)*, 2024, pp. 308–312. doi: 10.1109/ICEEICT62016.2024.10534440.

[2] S. M. Mahbub, A. A. M. Nafiz, A. A. Protiva, M. Tamim, and R. Rahad, “Ultra-short pulse: A comprehensive way of sensing pure solvents through hollow core photonic crystal fiber sensor,” *Opt Mater (Amst)*, vol. 156, p. 116028, 2024, doi: https://doi.org/10.1016/j.optmat.2024.116028.

[3] S. M. Mahbub, A. A. M. Nafiz, A. A. Protiva, and R. Hasan Sagor, “Sensing fuel adulteration level in diesel analyzing the change in shape of ultra-short pulse sent through Hollow Core Photonic Crystal Fiber,” 2024. [Online]. Available: https://ssrn.com/abstract=4765839

[4] S. M. Mahbub, A. A. M. Nafiz, and R. Hasan Sagor, “HC-PCF Refractive Index Sensor: Ultra-Short Pulse Propagation and Nonlinear Optical Phenomena,” Optik,2024. [Under Review]